

UNIVERSITY OF OTTAWA

MCG4322

RE3 - WILDCAT ENGINEERING

Capstone Report

Volume x of y

Joey Kane - 7386330

Isaak Goldenberg - 7395188

Sawyer Woodside - 7158568

Alex Pennell - 7334789

December 8, 2017



Sponsor: Dr. Eric Lanteigne

Abstract

- i. Contents of each book (if applicable)
 - ii. Description of design
 - iii. Special considerations
 - iv. Illustration of the final design
- half page, one paragraph

Contents

1	Introduction	1
1.1	Project Mandate	1
1.2	Group Problem Scope	1
1.3	Criteria and Restrictions	1
1.4	Parameterization Overview	1
2	Proposed Design	3
2.1	Gondola	3
2.1.1	Friction Wheel	6
2.1.2	Bearings	7
2.1.3	Linear Actuator	8
2.1.4	Door and Components	8
2.2	Keel	8
2.2.1	Thrusters	10
2.3	Wiring	14
3	Analysis	17
3.1	Outline	17
3.2	High Level Parametrization	17
3.3	System Modelling	17
3.4	Component Analysis	18
3.4.1	Thruster Assembly Component Selection	18
3.4.2	Thruster Shaft	18
3.4.3	Thruster Arms	18
3.4.4	Connection To Keel	18
3.4.5	Friction Wheel Slip	18
3.4.6	Bolt Compression Force	22
3.4.7	Linear Actuator	25
3.4.8	Gondola Arm Stresses	26
3.4.9	Bearing Mounting (Snap-Fit)	28
4	Discussion	31
A	Instructions for Installing and Running the GUI	37

B Code	39
B.1 Code 1	39
C Additional Material	45
C.1 Gondola Bearings	45
C.2 Gondola Arm Deflection	45
C.3 Gondola Arm Fatigue Failure	45
C.4 Thruster Motor	47
C.5 Thruster Arm Adhesion	47
C.6 Thruster Bearings	49
C.7 Gondola Motor Shaft	49
C.8 Vectoring Shaft Screw Axial Loading Conditions	49
C.9 Cauchy Stress Tensor [31]	50
C.10 Previous Drag Analysis	52
C.11 New Drag Analysis	54
C.12 Gondola Hinge	56
C.13 Thrust Force	57
D Data Sheets	65
D.1 Linear Actuator [1]	65
D.2 Bearings [20]	66
D.3 Friction Wheel Assembly	67
D.3.1 Friction Wheel [19]	67
D.3.2 Friction Wheel Set Screw [21]	68
D.3.3 Friction Wheel Motor [24]	69
D.3.4 Friction Wheel Encoder [25]	71
D.3.5 Example Cable Gland [17]	72
D.4 Spring [22]	74
D.5 Battery [8]	75
D.6 Thruster Assembly	76
D.6.1 Thruster Motor [15]	76
D.6.2 Propeller [13]	77
D.6.3 BESC [9]	78
D.6.4 Servo Motor [26]	79
D.6.5 Receiver [14]	81
D.7 Flight Control Assembly	82
D.7.1 ESC [10]	82

D.7.2 GPS Module [12]	83
D.7.3 Transceiver [16]	84
D.7.4 Flight Controller [11]	85
E Engineering Drawings	87
E.1 Parts List	87
E.2 Complete System Drawing	87
E.3 Sub-Assembly Drawings	87
E.4 Individual Part Drawings	87
F Meeting Minutes	89
F.1 Group Meeting Minutes	89
F.2 Team-Partner Meeting Minutes	97
G Recommendations for Improving the Course	99

List of Figures

1.1	Overview of Modelling Parametrization	2
2.1	Isometric View of the Gondola Assembly on the Keel	4
2.2	Partial Section of Gondola 1 (Components)	4
2.3	Gondola 1 Exploded View	5
2.4	Gondola Assemby on Curved Section of Keel	5
2.5	Linear Actuator Motion	6
2.6	Friction Wheel Interfacing with the Keel	7
2.7	Exploded View of the Friction Assembly	7
2.8	Overall Keel Assembly (Compressed)	9
2.9	Cross-Section of the Keel Connector	9
2.10	Connector Piece Assembling	10
2.11	Keel End Stop	10
2.12	Thruster Assembly on Thruster Arm	11
2.13	Overall Thruster Assembly	11
2.14	Mounting Plate Exploded View	12
2.15	Servo Mounting Exploded View	12
2.16	Shaft Mounting Exploded View	13
2.17	Propeller Bracket Mounting Exploded View	13
2.18	Propeller Exploded View	14
2.19	Gondola Component Wiring Schematic	15
2.20	Gondola Component Wiring	15
2.21	Thruster Wiring	16
2.22	Thruster Wiring	16
3.1	Parametrization Outline for the Friction Wheel Slip	19
3.2	Parametrization Outline for the Bolt Compression Force	22
3.3	Parametrization Outline for the Bolt Compression	25
3.4	Model Used to Compute the Deflection of the Gondola Arms	27
3.5	Centeroid of Section of Circle [32]	29
C.1	S-N Curve for Laser Sintered Nylon [3], Used to Determine the Fatigue Failure of the Gondola Body	46
C.2	Analysis of Carbon Fibre Adhesion (From Shigley's Machine Design [5, 484])	47
C.3	HS-7950TH Servo Spline Attachment [27]	49

C.4 Drag Force Curves Computed From SolidWorks Flow Simulation	52
C.5 Drag Force Curves Computed From SolidWorks Flow Simulation	53
C.6 Gondola Hinge Comparison Fillet Vs. No Fillet	56
C.7 Graph of Thrust Plotted Against Airship Speed at 11000rpm With 7", 5" Pitch Diameter Propeller	60
C.8 Test Data from Gabriel Staples Against Experimental Static Thrust Values [29]	61
C.9 Test Data from Gabriel Staples Against Experimental Dynamic Thrust Values [29]	62
C.10 Sample Thrust Calculation Using On-line Calculator [7]	63

List of Tables

3.1	List of All Parametrized Components	17
3.2	List of All Inconsequential Analysis	17
C.1	Table of Bolt Strength for a M3-0.5 Bolt [2]	50
C.2	Raw Data From SolidWorks Flow Simulation	52
C.3	Airship Model Characteristics and Data [30]	54
C.4	Drag Contribution for Various Airship Components [30]	55
C.5	Fineness Ratios and Corresponding C_D	56
C.6	Table of Calculated Thrust Values for Varying Airship Speeds	59
D.1	Various Gearing For Gondola Motor Torque [24].	70

Nomenclature

E_p	Modulus of elasticity of considered plastic hub or boss [N/mm^2]
F_R	Keel to assembly arm connector reaction, [N]
F_T	Thruster force, [N]
F_g	Force of gravity, [N]
F_{GR}	Reaction force of gondola, [N]
F_{K1}	Keel reaction force 1, [N]
F_{K2}	Keel reaction force 2, [N]
F_{LA}	Linear actuator force, [N]
F_{NB}	Normal force applied to bearing, [N]
F_{RSF}	Force of snap fit bearing [N]
F_α	Force on fastener α (hinge to gondola), [N]
F_β	Force on fastener β (hinge to gondola), [N]
F_a	Force on fastener a (hinge to gondola), [N]
F_{bolt}	Bolt pretension force, [N]
F_{brake}	Normal braking force keel reaction, [N]
F_b	Force on fastener b (hinge to gondola), [N]
F_{c1}	Connector moment couple force 1, [N]
F_{c2}	Connector moment couple force 2, [N]
F_{ffric}	Friction force acting on friction wheel, [N]
F_{nfric}	Normal force acting on friction wheel, [N]
F_{s1}	Force on friction wheel motor fastener 1 , [N]
F_{s2}	Force on friction wheel motor fastener 2 , [N]
F_{spring}	Force applied by hinge spring, [N]
H_{keel}	Height of the bearing arm contact point on the keel, [m]

L_G	Width of gondola, [m]
L_a	Length from pivot point of hinge to fastener a , [m]
L_b	Length from pivot point of hinge to fastener b , [m]
L_m	Length from side of gondola to gondola drive motor hinge, [m]
L_s	Length from fastener to fastener of gondola motor to hinge, [m]
L_{SF}	Length to snap fit bearing, [m]
L_{ac}	Length from centerline of gondola to fastener a, [m]
L_{bc}	Length from centerline of gondola to fastener b, [m]
L_{cm}	Length from gondola wall to center of mass of gondola, [m]
$L_{contact}$	Length from contact to contact of bearings on keel, [m]
L_{drive}	Length of gondola hinge to friction wheel contact, [m]
L_{hs}	Distance from the pivot of the hinge to the gondola motor fastener, [m]
L_{hw}	Distance from the gondola motor fastener to the contact point of the friction wheel, [m]
L_{rx}	Friction wheel motors shaft length, [m]
M_1	Reaction moment on bearing arm, [Nm]
M_R	Connector moment reaction, [Nm]
R	Reaction force, [N]
$S_{compressive}$	Compressive strength of gondola material, [Pa]
T_w	Friction wheel motor torque, [Nm]
T_{spring}	Torque of hinge spring, [Nm]
W_A	Weight of thruster assembly arm, [N]
W_E	Weight of thruster enclosure, [N]
W_T	Weight of thruster, [N]
W_c	Weight of connection piece, [N]
W_{LA}	Weight of linear actuator, [N]

η	Safety Factor
μ	Coefficient of friction
σ'	Von Mises Stress, [Pa]
σ_{washer}	Compressive force of washer, [Pa]
σ_x	Principle stress, [Pa]
σ_a	Hoop stress, [N/mm ²]
σ_s	Allowable design stress for plastic, N/mm ²
$a_{airship}$	Acceleration of airship, [m/s]
$a_{gondola1}$	Acceleration of Gondola 1 , [m/s ²]
$a_{gondola2}$	Acceleration of Gondola 2 , [m/s ²]
c	Distance from neutral axis to stress location, [m]
d_i	Interference diameter, [mm]
d_s	Hub outer diameter, [mm]
d_s	Shaft diameter, [mm]
i_a	Allowable interference, [mm]
$m_{airship}$	Mass of airship, [kg]
$m_{gondola1}$	Mass of Gondola 1, [kg]
$m_{gondola2}$	Mass of Gondola 2, [kg]
r_{fw}	Radius of friction wheel, [m]
w_{armx}	Width of the bearing arm in the x direction, [m]
w_{army}	Width of the bearing arm in the y direction, [m]

Chapter 1: Introduction

1.1 Project Mandate

The goal of the project is to overcome the current limitations involved with the control and landing of unmanned airships in adverse outdoor conditions. The airship consists of a helium filled envelope, external keel, and gondola which will act as a ballast. The moving ballast will control the pitch by the controlled displacement of the centre of mass. Propulsion will be provided by propellers in the X-Y plane of the airship. The system will have vector thrusting to allow for altitude change independent of pitch change.

1.2 Group Problem Scope

The research project led by Dr. Eric Lanteigne involves designing a system to allow for the control of an unmanned airship. The goal of the project is to create a system that controls the airship by changing the position of the centre of mass to initiate pitch change. This pitch change, along with forward propulsion, will drive the airship in a given direction. The design team will be responsible for creating a system, where a gondola that acts as a ballast, will move along a non-linear, diamond-shaped keel in order to initiate pitch change of an airship. Ideally, the system will be able to incur a pitch change of up to ninety degrees, allowing the airship to descend straight downwards. Currently, all designs must be scalable as specifications of the airship envelope have yet to be finalized. The unmanned airship must be capable of flying outdoors and be able to carry a payload of between 0.2kg and 0.5kg. The main components of the design can be split up into: Gondola Design, Gondola Movement, Securing Gondola to Keel, Gondola Position Measurement, Securing the Propellers, Thrust Vectoring, Batteries, and Wire Management.

1.3 Criteria and Restrictions

The propellers will be in the X-Y plane, in line with the centre of volume. This eliminates any moments from the propellers that lead to imbalance and unwanted pitch variations. The gondola will be able to move along the varying curvature of the keel using a hinged-gondola. The driving mechanism will be two friction wheels with the additional support of 4 driven bearings. The cross-section of the keel is diamond-shaped, however it is not torsionally constant, therefore the vertexes are not coincident on the curved section. Once the airship has been constructed, a Special Flight Operations Certificate (SFOC) issued by Transport Canada will be necessary in order to fly the airship lawfully.

1.4 Parameterization Overview

A high level overview of the system's parametrization is shown in Figure 1.1.

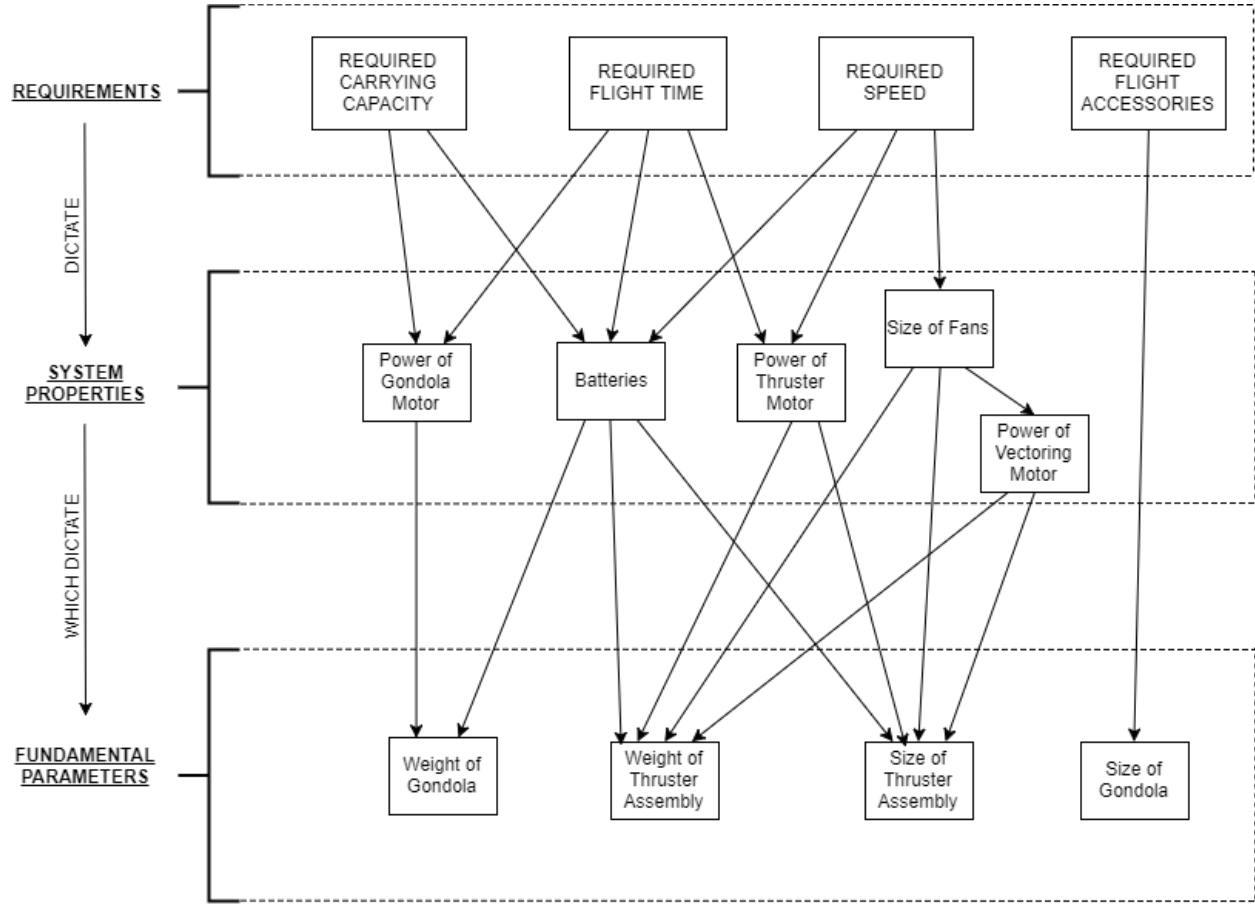


Figure 1.1: Overview of Modelling Parametrization

Figure ?? is a more detailed parametrization outline, which shows how user inputs will be converted to forces using an iterative approach. This approach will be used to compute all forces shown in Section ADD HERE??.

Once all of the forces acting on the body are computed, failure analyses for each part are conducted in Section ADD HERE.

Chapter 2: Proposed Design

Introduction Paragraph

2.1 Gondola

The gondola sub-assembly is the most distinguishable feature of the airship design. The gondola moves along the keel in order to rapidly pitch the airship. The assembly can be seen in Figure 2.1. Movement along the gondola is driven by two friction wheels which interface with the cover on the keel through the friction between the two surfaces. Bearings are used as wheel to hold the gondola on top of the keel, while the friction wheel are in contact with the bottom edge of the keel. The gondola is comprised of two half sections which each house components, such as the battery, flight controller, transmitter, GPS module and two ESCs. Figure 2.2 shows how these components are nested one of the gondola sections. Joining the two sections is a hinge, seen in Figure 2.3, which allows the gondola to bend in the centre. The bend in the middle allows the gondola to overcome a more significant turning radius compared to being fixed in a straight line, which is depicted in Figure 2.4. Similarly to curve fitting, the more points that are used, the better fit. Braking of the gondola is accomplished by turning the friction wheels in the opposite direction and the position is held by a linear actuator, which provides force perpendicular to the keel surface. The linear actuator motion can be seen in Figure 2.5. The gondola has been designed to be resistant to small amounts of water, considering the gondola will always be shielded from rainfall by the envelope, therefore total waterproofing is not required. Cable glands will be used for all surfaces perpendicular to rainfall that require waterproofing. They can be seen in Figure 2.3. The gondola section are made using high quality 3D prints, given their complex geometries and relatively small size.

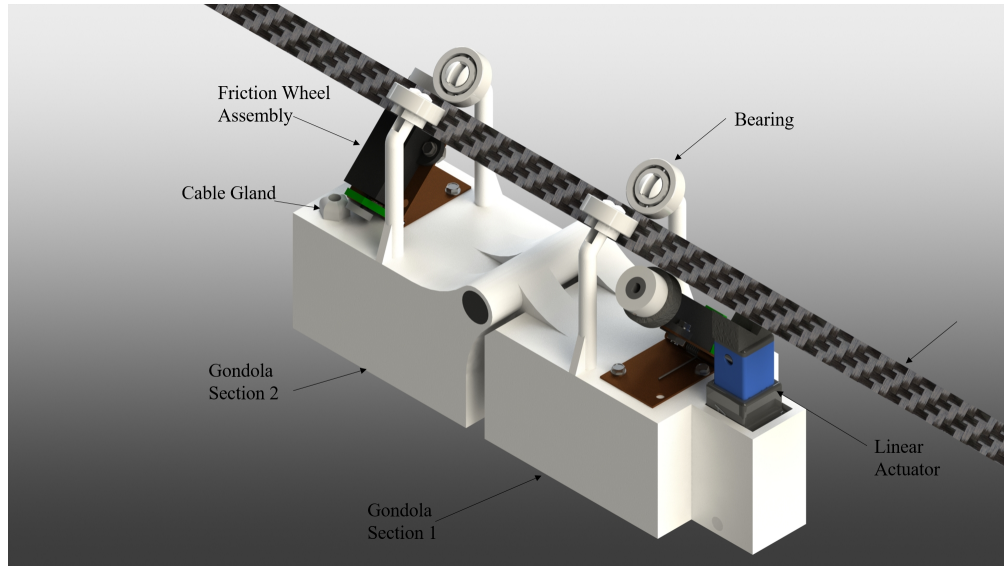


Figure 2.1: Isometric View of the Gondola Assembly on the Keel

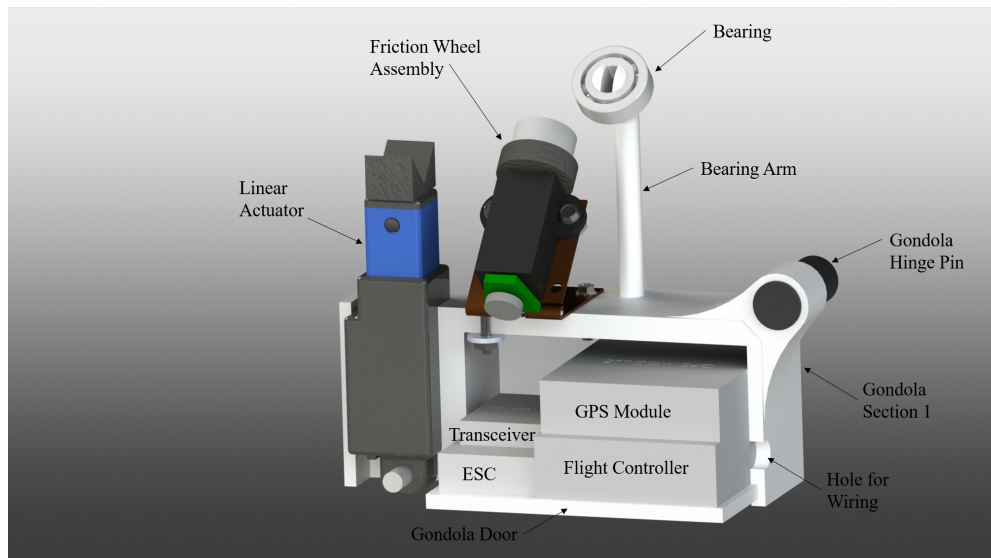


Figure 2.2: Partial Section of Gondola 1 (Components)

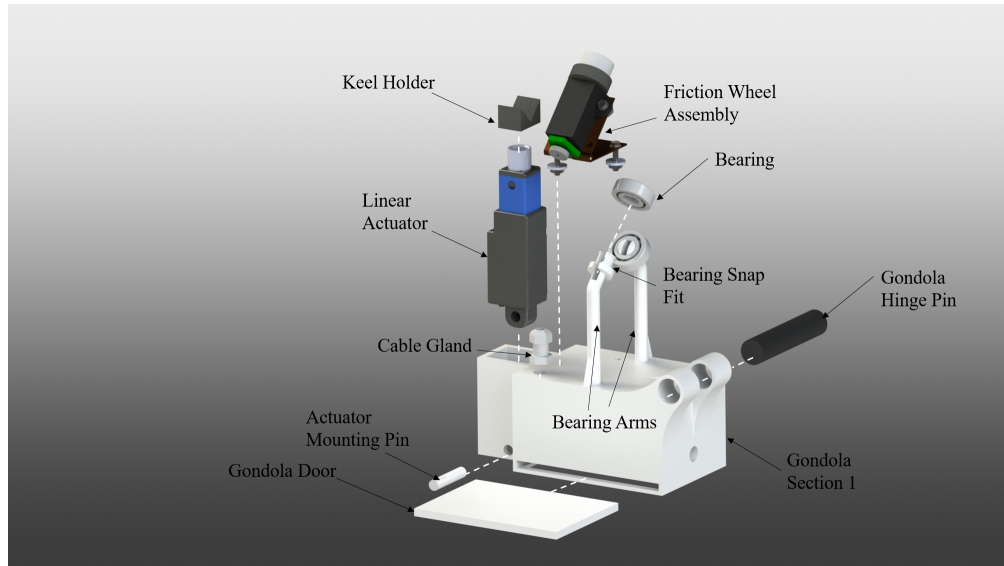


Figure 2.3: Gondola 1 Exploded View

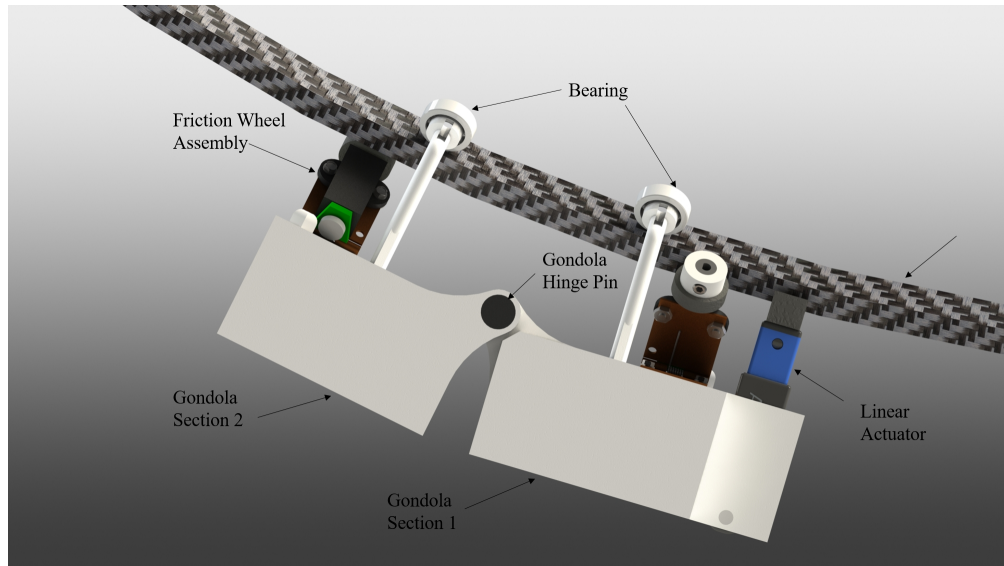


Figure 2.4: Gondola Assembly on Curved Section of Keel

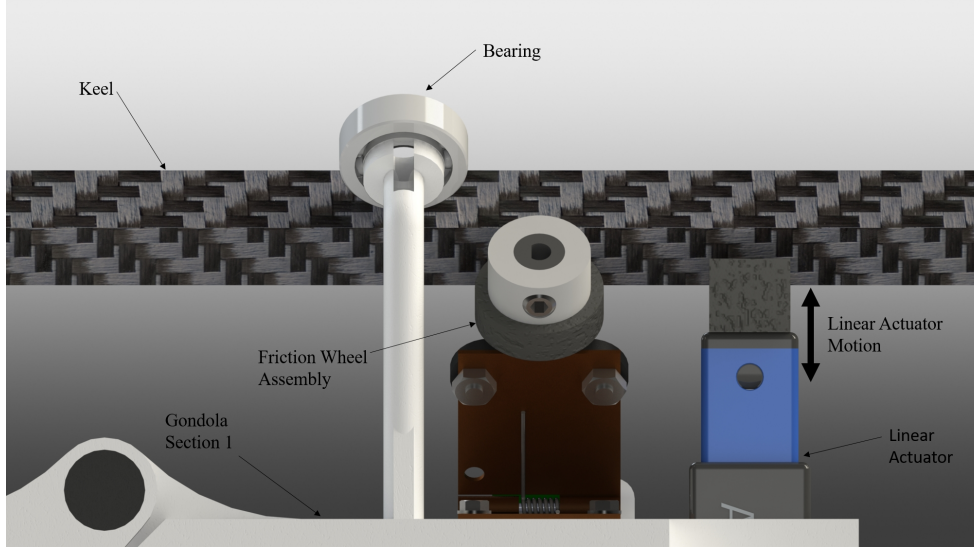


Figure 2.5: Linear Actuator Motion

2.1.1 Friction Wheel

The friction wheel must always be in contact with the keel, shown in Figure 2.6. The friction wheel is made from 55D rubber, purchased off-the-shelf so it can deform when it is placed on the keel. A shaft adapter is necessary to bridge the gap between the motor shaft and the friction wheel, as the two sizes are not compatible. The shaft adapter will be 3D printed, and held in place by an existing set screw in the friction wheel. To ensure adequate pressure on the keel, the friction wheel assembly is mounted on a hinged bracket equipped with a torsion spring at the pin, as seen in Figure 2.7. The motor used can rotate in both directions, making it useful as a brake also. A magnetic encoder allows for accurate positioning of the gondola sections, independently allowing for redundancy between the two motors. The motor is mounted to the bracket using two nuts and two bolts. The bracket is mounted to the gondola using 2 nuts, 2 bolts and 2 washers. The bracket and hinge will be manufactured in house with a sourced torsion spring.

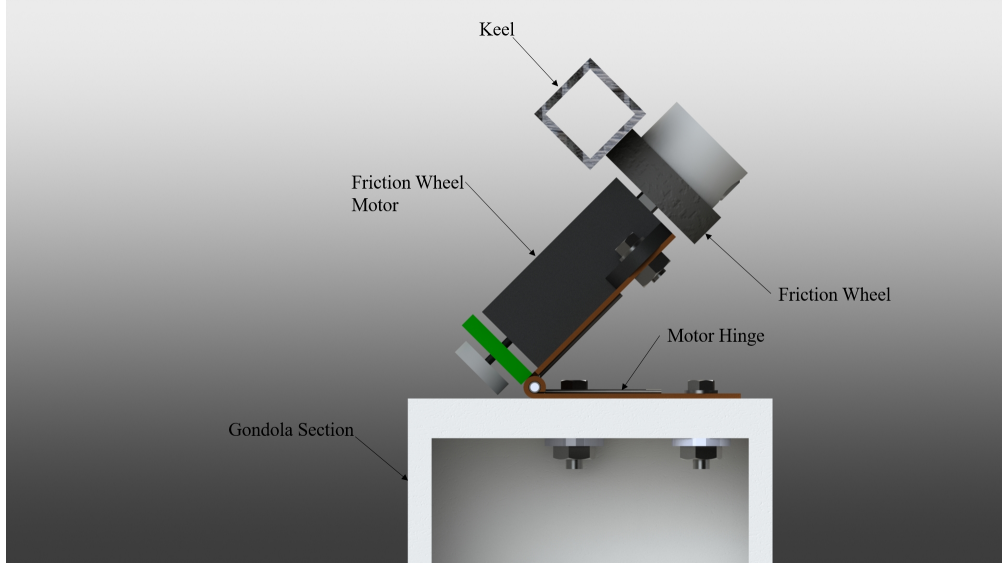


Figure 2.6: Friction Wheel Interfacing with the Keel

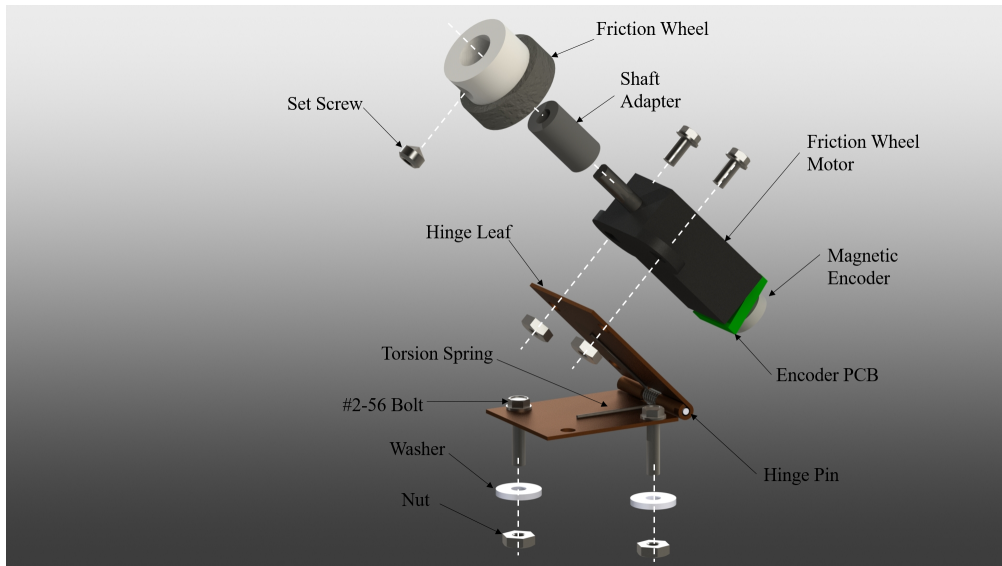


Figure 2.7: Exploded View of the Friction Assembly

2.1.2 Bearings

Bearings are placed on top of the keel to support the weight of the gondola and counter the force applied to the keel by the friction wheel. The bearings act as wheels turning and slipping along the keel. Low weight, plastic bearings will be used. The bearings are mounted using a snap fit design, that can be seen in 2.3, where the bearing is held in place by a diameter slightly larger than its own. The bearing is placed over the piece, deflecting it until the bearing can slip past the overhang where the snap fit piece elastically snaps back into its original position, securely holding the bearing.

2.1.3 Linear Actuator

A linear actuator is housed on one of the two sections of the gondola. The linear actuator is to be activated when the gondola is not moving to hold its position on the keel. The motion can be seen in Figure 2.5 A custom 3D printed piece is outfitted to the top of the actuator (Keel Holder) in a V-shape to mesh ideally with the keel, as seen in Figure 2.3. The V-shaped 3D printed surface will then be coated with a Plasti Dip® like coating, to reduce the likelihood of tearing the polyurethane cover on the keel. The linear actuator chosen has a holding force of 45N without constant power, making it ideal for run time. It is also water resistant to the IP54 standard.

2.1.4 Door and Components

The gondola features a sliding door (the motion can be seen in Figure 2.3), to ease the process of component charging and changing. The door relies upon an interference fit to stay in place and components are placed on top of the door once it is half closed. See Figure 2.2 (selective cross-section). The door will be 3D printed also.

2.2 Keel

Figure 2.8 shows the keel assembly in a condensed form. The two straight and one curved sections of the keel and the envelope support originate from Dr. Lanteigne's design. Sections of the keel are joined using connectors that rely on interference fits, also designed by Dr. Lanteigne, but modified and machined for better material properties. The envelope support slides into a slot on the keel connectors remaining in position by bottoming out. Thrusters are mounted on carbon fibre arms that also slide into the connector, maintaining position by bottoming out as well. The section shown in Figure 2.9 displays the bottoming out and Figure ?? shows the fit. 3D printed end stops are inserted in either end of the keel using an interference fit identical to the connectors. The end stop design can be seen in Figure 2.11. These stops are slightly larger than the size of the keel, effectively interfering with the gondola wheels, keeping it from rolling off the ends of the keel. All geometries in the keel assembly are fixed in relation to the airship with the exception of the thrusters.

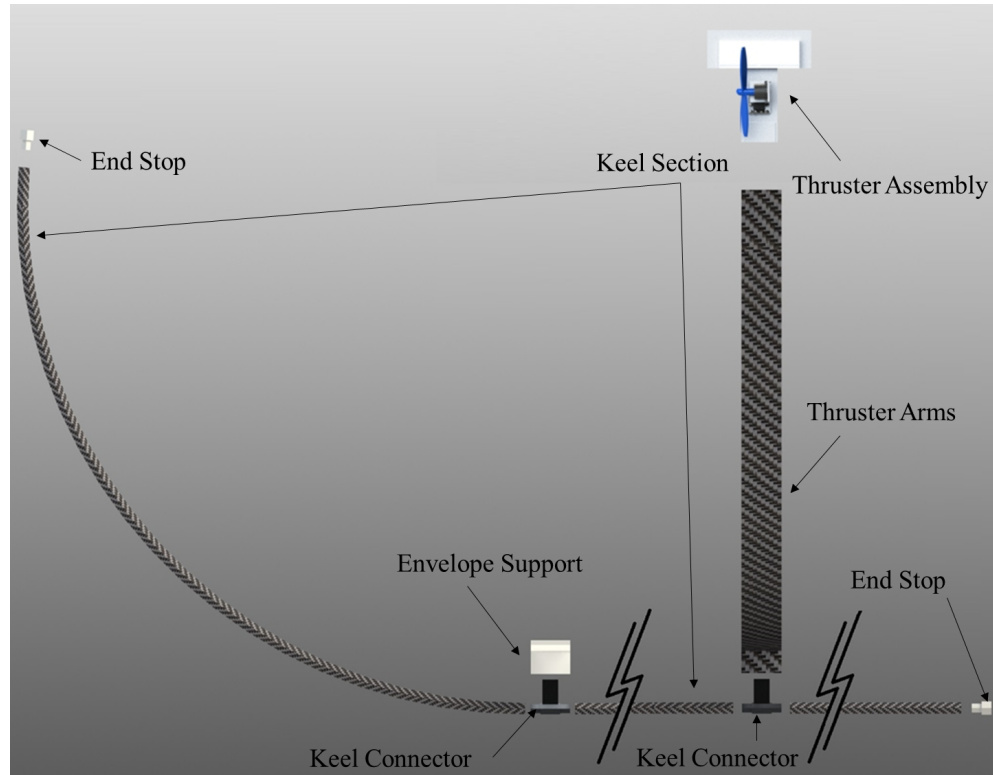


Figure 2.8: Overall Keel Assembly (Compressed)

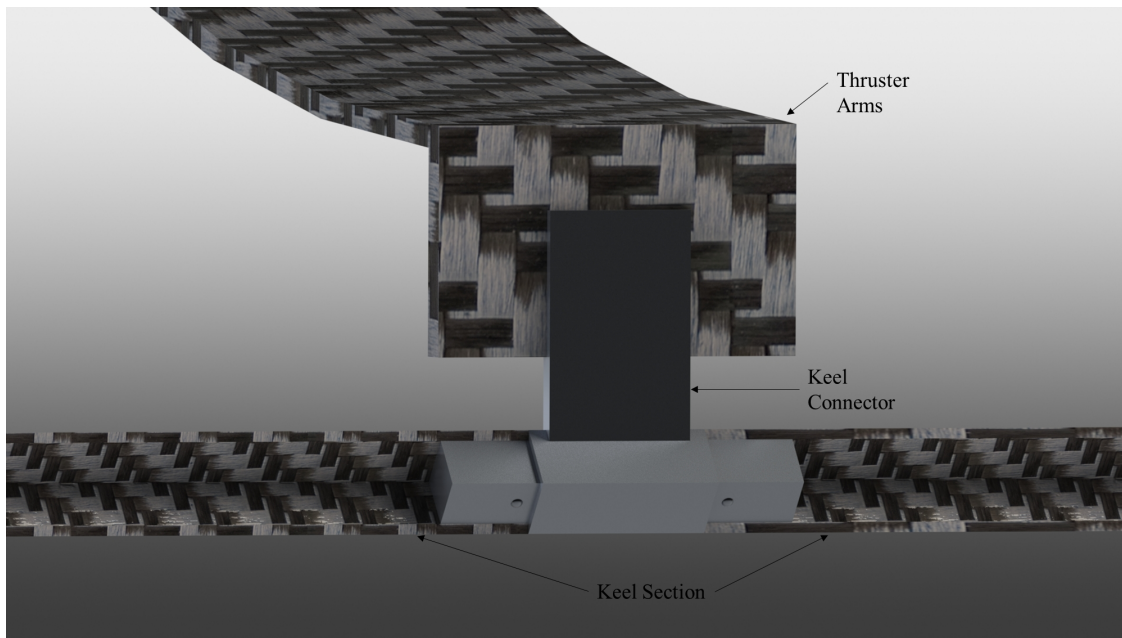


Figure 2.9: Cross-Section of the Keel Connector

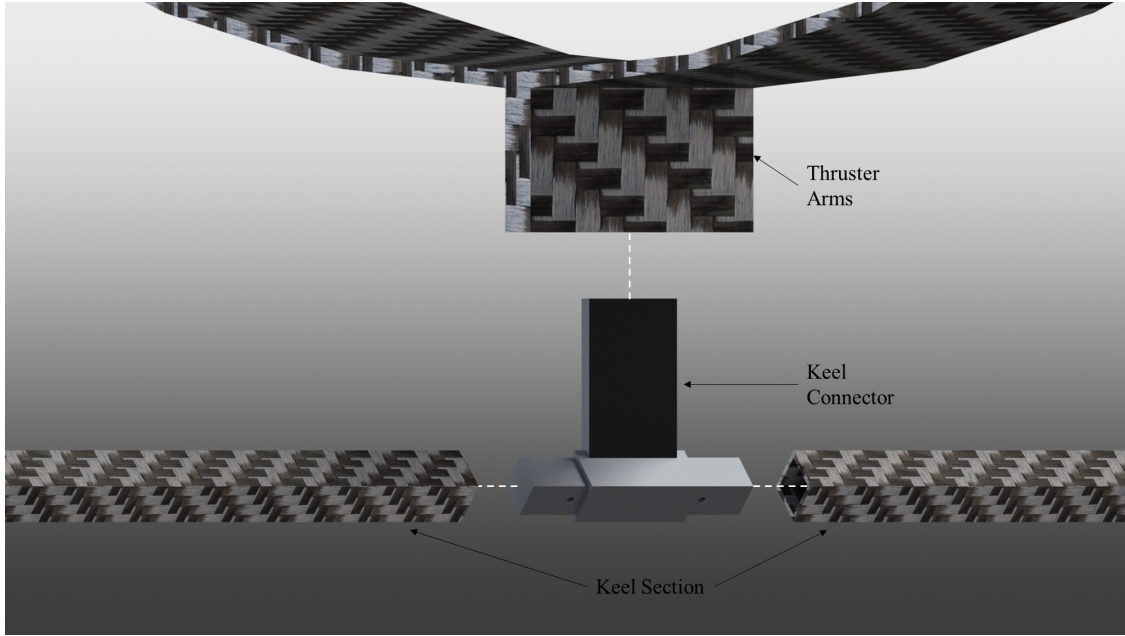


Figure 2.10: Connector Piece Assembling

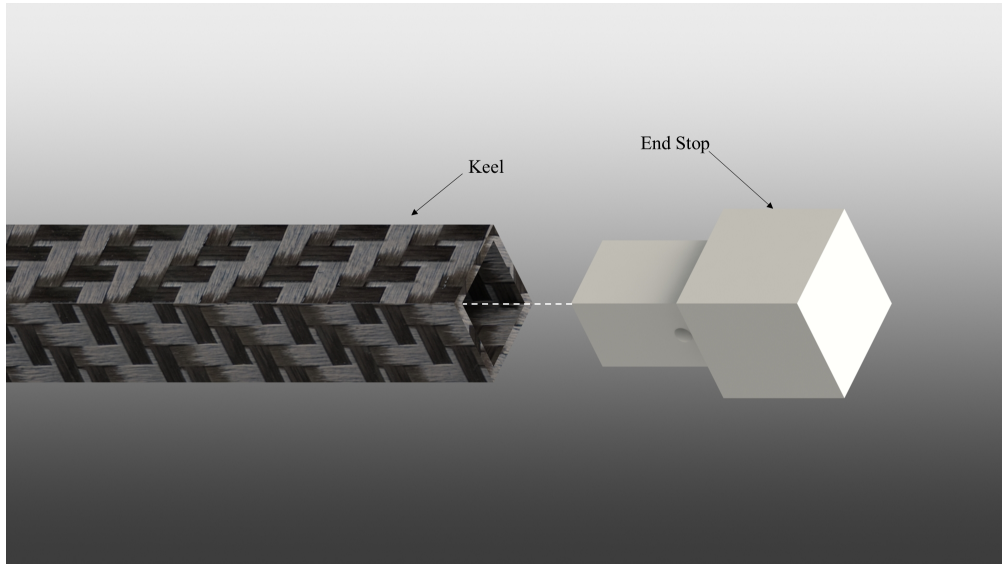


Figure 2.11: Keel End Stop

2.2.1 Thrusters

The thruster arms are made from carbon fibre that will be made in house by laying sheets of carbon fibre on a balloon mold. A CNC machined aluminum plate is attached to the U-shaped carbon fibre arms by welding a machined cap piece onto the plate, then inserting the carbon fibre arm into it and applying epoxy. This mounting technique can be seen in Figure 2.12. The full assembly can be seen in Figure 2.13. Components are housed inside a 3D printed casing that features a 3D printed door, similar to the gondola.

Figure 2.14 displays how the components are mounted on the plate. The components for each thruster include, a receiver, a battery and a BESC. The components are located above the centre of volume of the airship in the z-direction, raising the centre of mass. These components are well covered from the rain and any splashing water. With the casing above the servo motor, the servo motor is shielded from rain in normal flying conditions.

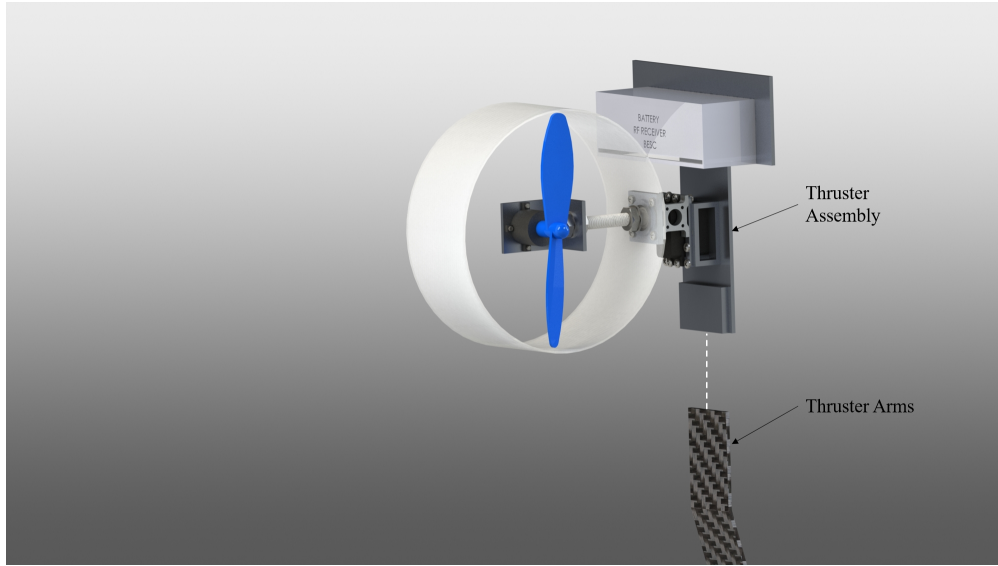


Figure 2.12: Thruster Assembly on Thruster Arm

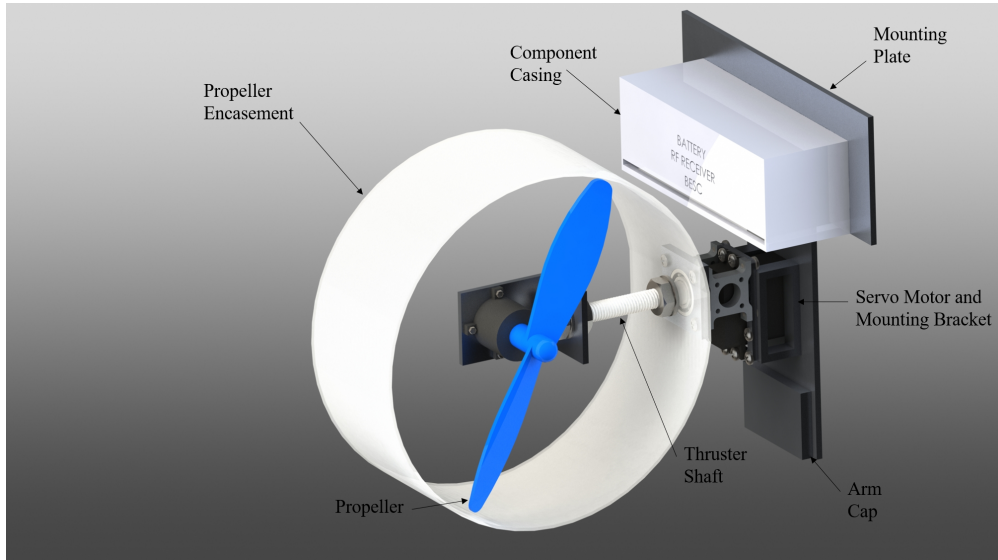


Figure 2.13: Overall Thruster Assembly

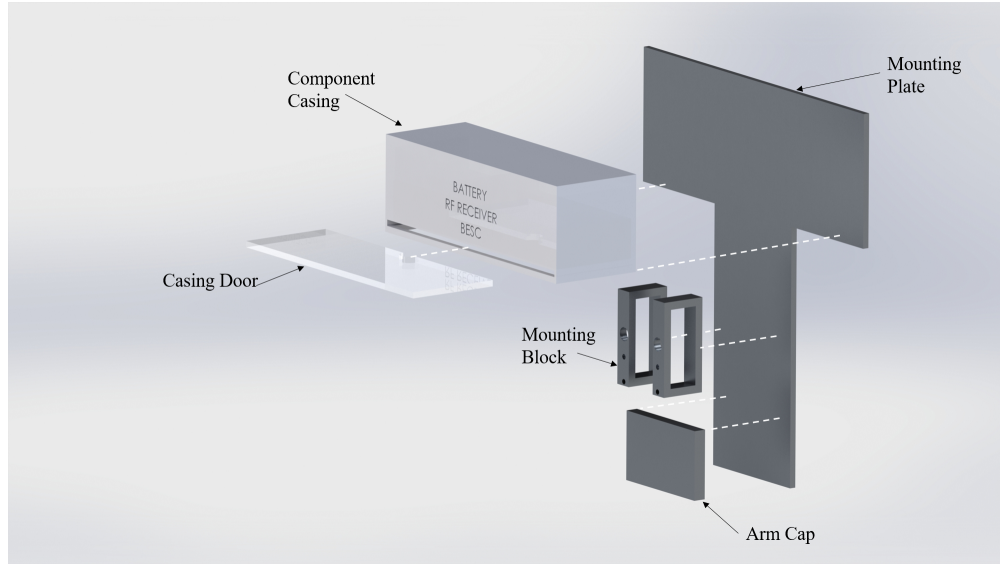


Figure 2.14: Mounting Plate Exploded View

A servo motor is mounted to the plate using aluminum blocks along with off-the-shelf assembly, as seen in Figure ???. A bearing and custom machined bracket are added to the off-the-shelf to support the shaft attached to the servo motor. Figure 2.16 shows the bearing racket, bearing and shaft. The shaft will be machined to hollow, threaded on the outside and a shoulder that fits into the bearing inner race. The shaft is mounted to the spline on the servo, and an M3 screw is placed inside to shaft, axially fastening it to the servo, as the servo comes standard with a tapped hole. Several screws are used to securely fasten the servo to the supporting parts.

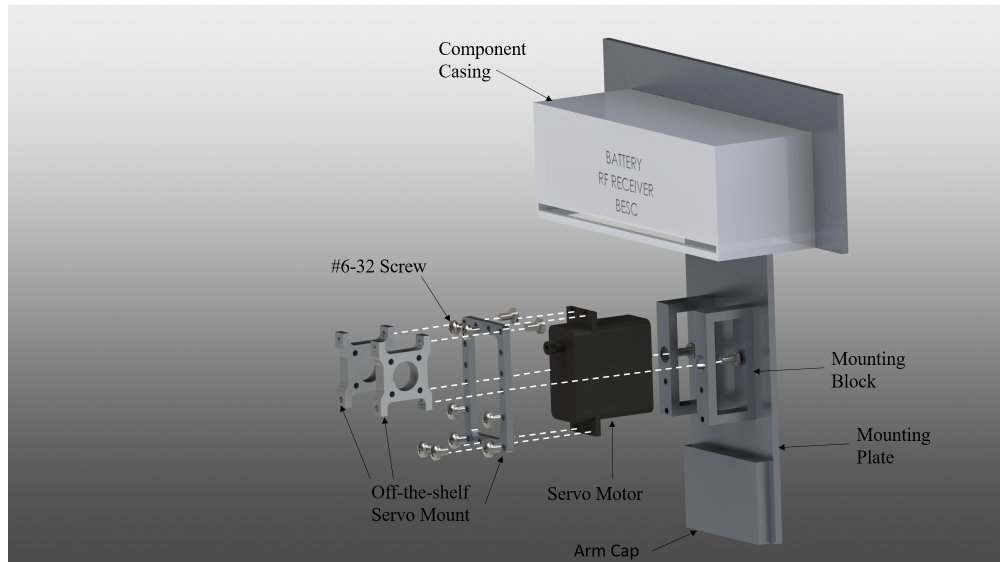


Figure 2.15: Servo Mounting Exploded View

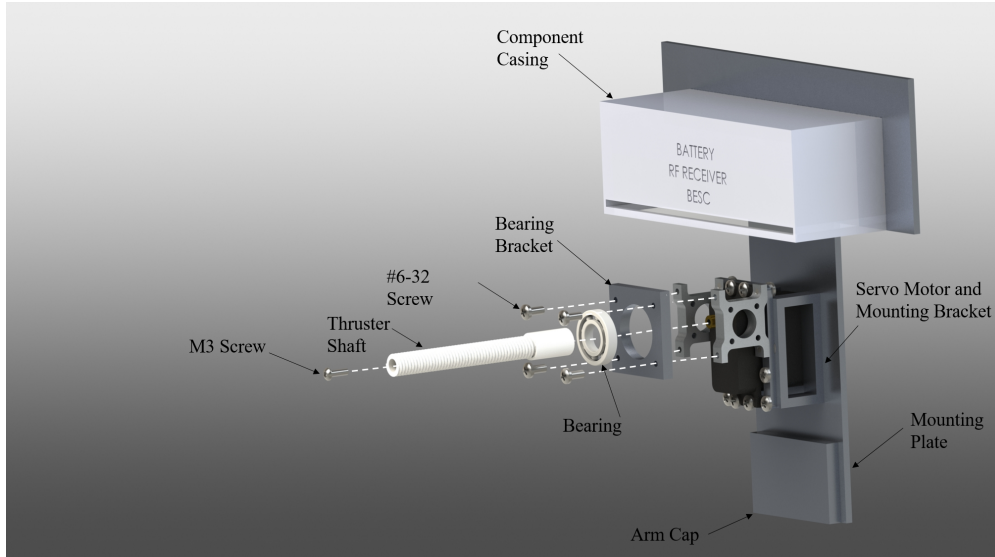


Figure 2.16: Shaft Mounting Exploded View

The propeller motor is mounted on a machined propeller mounting bracket with tapped holes using screws, which is mounted on the shaft using washers and nuts. Figures 2.17 and 2.18 show how the propeller and related parts will be mounted. The propeller is mounted to the motor using a standard interference fit, given that these are both off-the-shelf parts. The propeller and motor are protected by a lightweight encasement (MANUFACTURED HOW????) that is mounted to the shaft by squeezing the plastic between a shoulder on the shaft and washer/nut combination. The encasement provides shielding of the propeller motor during forward flight conditions.

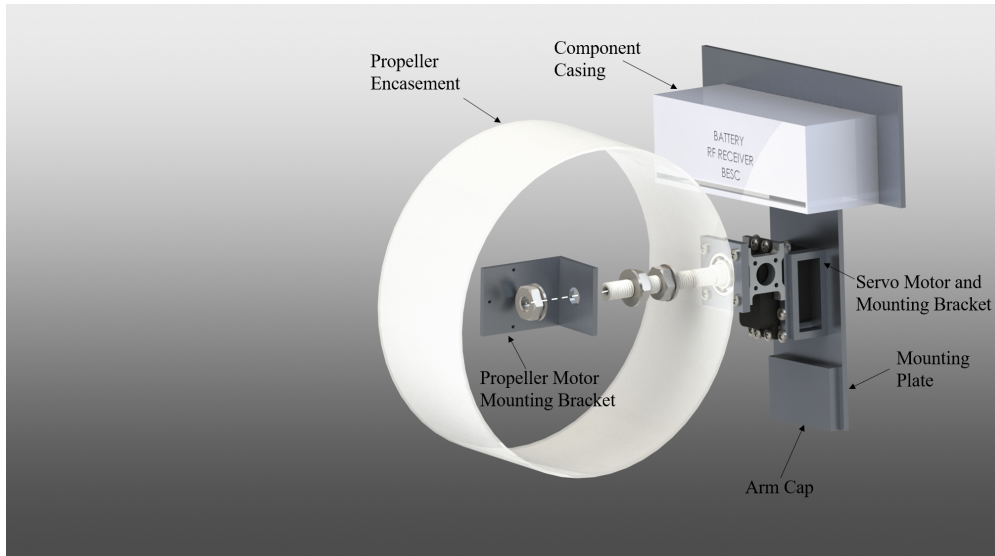


Figure 2.17: Propeller Bracket Mounting Exploded View

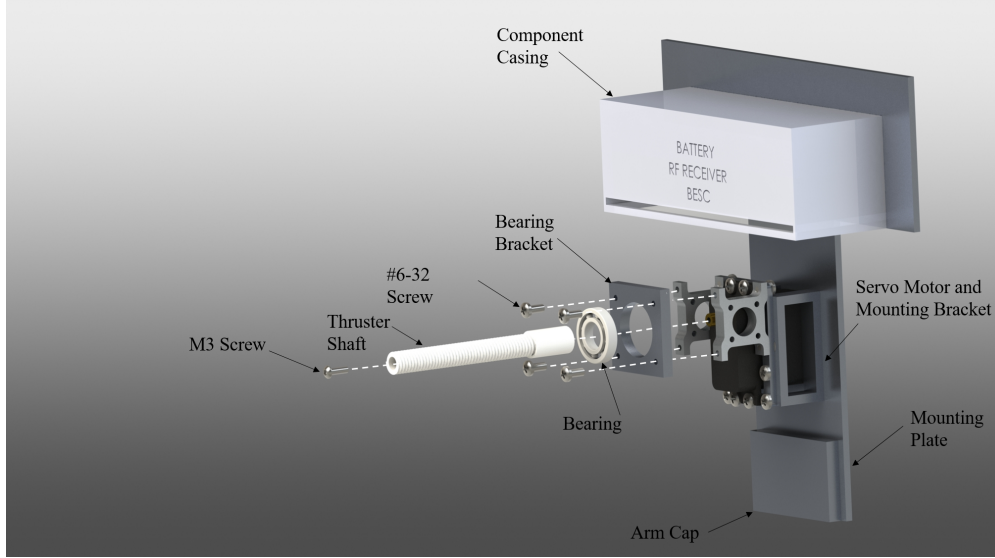


Figure 2.18: Propeller Exploded View

2.3 Wiring

Wiring for the airship is relatively straight forward as each motor assembly has an independent power supply. Transmitters and receiver eliminate the need for wiring throughout the airship. Avoiding communication wiring significantly reduces the likelihood of wires tangling and causing jamming of parts. For the gondola, Figure 2.20 shows how wires will be routed. Components shown are rough dimensions taken from the specifications for each part, and include the start of the tails of the wires. Waterproofing is provided by cable glands for surfaces perpendicular to the fall of rain. Surfaces parallel to the fall of rain do not have waterproofing as these are not exposed to much water. The wires routed between the gondola will be provided with slack so the gondola can fold up to 10°.

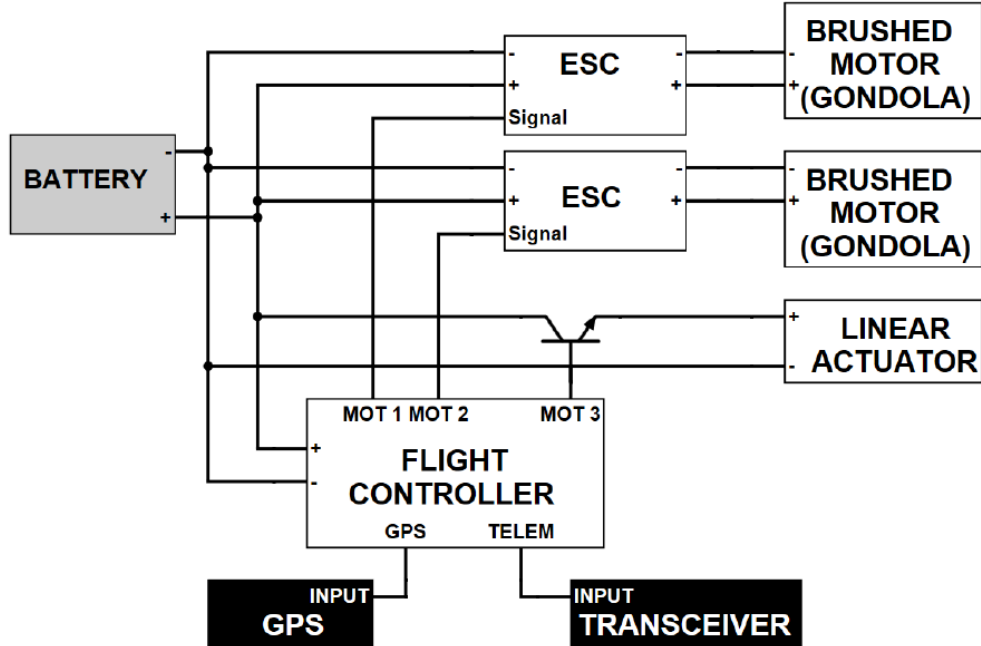


Figure 2.19: Gondola Component Wiring Schematic

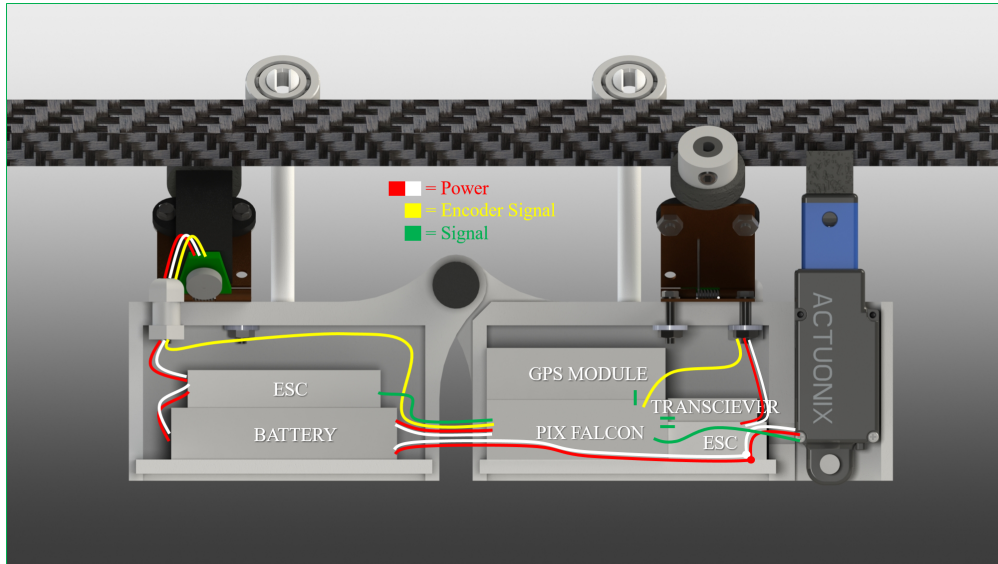


Figure 2.20: Gondola Component Wiring

The thruster assembly is wired similarly to the gondola, with wires coming out of the component casing. The wire is then routed through the thruster shaft. Figure 2.22 shows a diagram of the thruster wiring. Waterproof cannot be completed for the propeller motor as it must be exposed to the air to work effectively. Although the propeller motor is not waterproofed, it is cover by falling rain from the propeller encasement in forward flight operations.

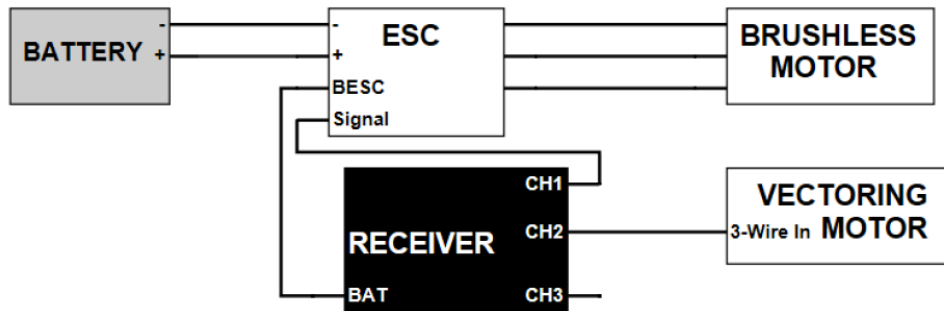


Figure 2.21: Thruster Wiring

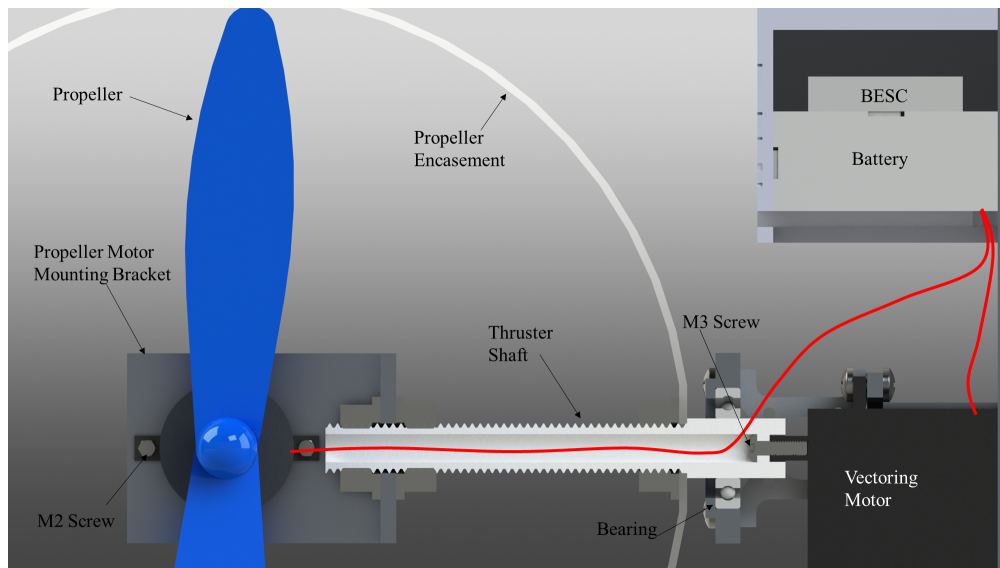


Figure 2.22: Thruster Wiring

Chapter 3: Analysis

3.1 Outline

Table 3.1: List of All Parametrized Components

Section	Analysis	Parametrized Part	Failure Likelihood
3.4.1	Thruster Assembly Component Selection	Thruster Battery	MEDIUM
		Propeller Diameter	
		Motor	
		Thruster Shaft Length	
		Diameter of Encasement	
3.4.2	Thruster Shaft	Diameter of Thruster Shaft	MEDIUM
		Thread Type	
		Material Type	
		Bearing Dimensions	
3.4.3	Thruster Arms	Width	HIGH
		Thickness	
3.4.4	Connection To Keel	Width of Insert	HIGH
3.4.5	Friction Wheel Slip	Spring Force	MEDIUM
		Motor Torque	
3.4.6	Gondola Hinge Bolts	Diameter of Washers	MEDIUM
3.4.9	Gondola Bearing Snap-Fit	Depth of Cut	HIGH
		Distance of Arms from Keel	

Table 3.2: List of All Inconsequential Analysis

Section	Inconsequential Analysis	Failure Likelihood
C.1	Gondola Bearings	LOW
C.2	Gondola Arm Deflection	LOW
C.3	Gondola Arm Fatigue	LOW
3.4.8	Gondola Arm Stresses	LOW
C.4	Thruster Motor	LOW
3.4.7	Linear Actuator	LOW
C.6	Thruster Bearings	LOW
C.5	Thruster and Arm Adhesion	LOW
C.8	Vectoring Motor Shaft Axial Loading	LOW

3.2 High Level Parametrization

3.3 System Modelling

worst case scenarios here

3.4 Component Analysis

3.4.1 Thruster Assembly Component Selection

3.4.2 Thruster Shaft

3.4.3 Thruster Arms

3.4.4 Connection To Keel

3.4.5 Friction Wheel Slip

The friction wheel slip analysis, calculates the required motor torque in order to allow for the gondola to move in a worst case scenario, and then calculates the motor hinge spring torque that will generate a large enough normal force to prevent slip of the friction wheel. The inputs required for the analysis are the geometry of the friction wheel, the motor, the hinge, the gondola, as well as the material properties of the friction wheel, the mass of each gondola car, the maximum achievable thruster acceleration and the loading conditions specific to the worst case scenario.

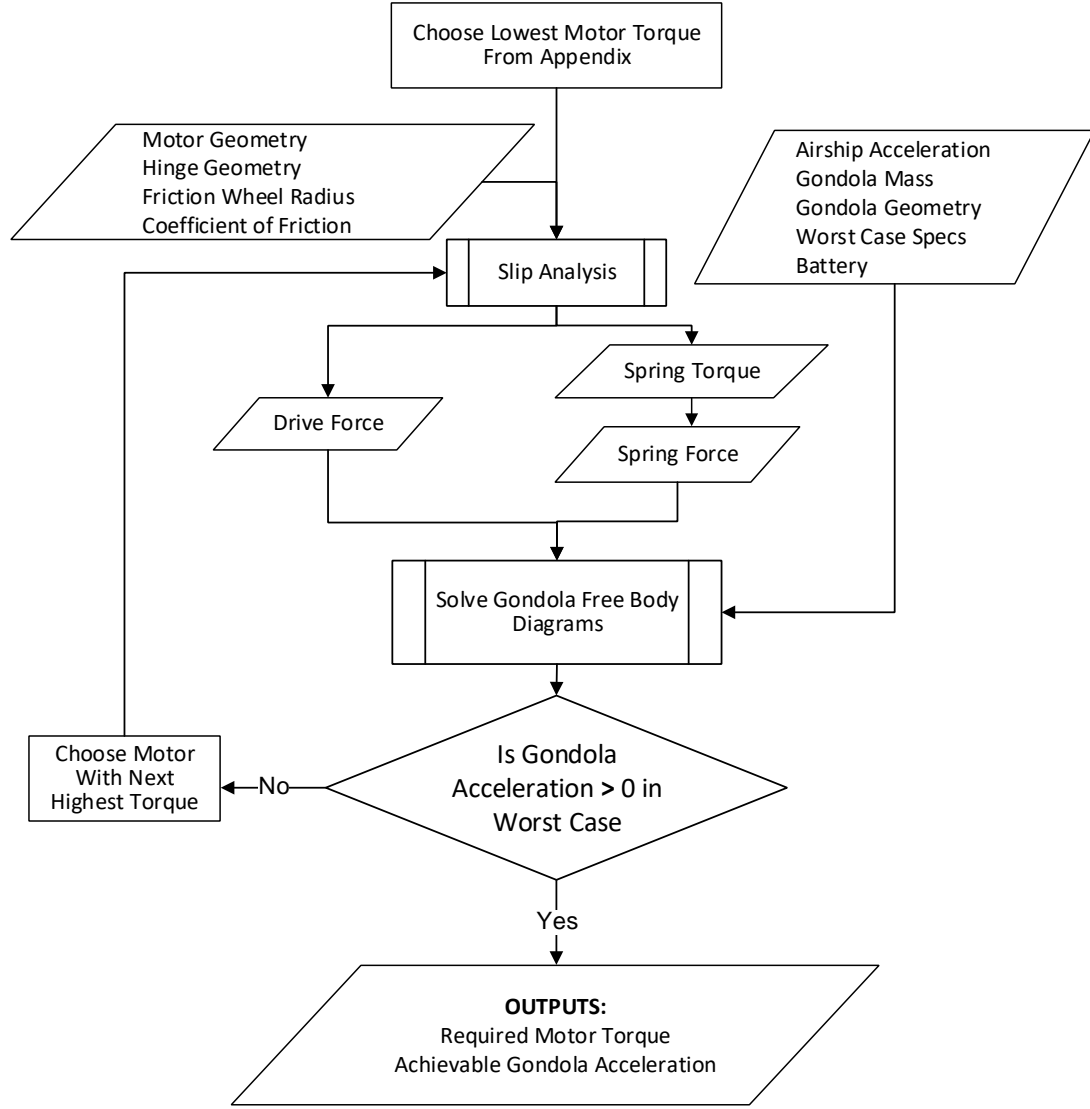


Figure 3.1: Parametrization Outline for the Friction Wheel Slip

The friction wheel slip analysis, calculates the required motor torque in order to allow for the gondola to move in a worst case scenario, and then calculates the motor hinge spring torque that will generate a large enough normal force to prevent slip of the friction wheel. The inputs required for the analysis are the geometry of the friction wheel, the motor, the hinge, the gondola, as well as the material properties of the friction wheel, the mass of each gondola car, the maximum achievable acceleration as a result of the thrusters and the loading conditions specific to the worst case scenario.

Parameters that will not change through out the gondola analysis include, the geometry of the motor, this is because different torques can be achieved with the same geometry by modifying the gearing. See Appendix D.3.3. The geometry of the hinge will not change as it is aluminium and the forces applied to it are

minimal. The components inside of the gondola which include the R.F transmitter, the BESC and the battery will not be changing. Calculations for required power and run time are done in APPENDIX***** show that regardless of motor gearing, power requirements are easily met and the limiting factor for flight time will be the thruster batteries. As a result the geometry of the main frame of the gondola (length, width, and height) will not be parameterized and the weights of the gondola will remains approximately the same.

The analysis first assumes a motor torque. With this torque the code computes the spring torque such that $F_{spring} = F_{Nfric}$, which ensures the friction wheel will not slip. For the purpose of this analysis, the friction wheel and shaft interface are considered without slip, and the set screw is assumed to not fail as it will be metal interfacing with plastic.

$$F_{spring} = F_{Nfric} = \frac{F_{fFric}}{\mu} = \frac{T_w}{r_{Fw} \cdot \mu} \quad (3.1)$$

$$F_{spring} = \frac{T_{spring}}{L_{hs} + L_{sw}} \quad (3.2)$$

$$\frac{T_{spring}}{[L_{hs} + L_{sw}]} = \frac{T_w}{r_{Fw} \cdot \mu} \quad (3.3)$$

The relation for the minimum necessary spring torque is multiplied by a factor of 1.5 in order to account for any neglected external factors.

$$T_{spring} = \frac{T_w \cdot [L_{hs} + L_{sw}]}{r_{Fw} \cdot \mu} \cdot 1.5 \quad (3.4)$$

Based on the assumed torque and the spring force, the acceleration of the gondola in the worst case scenario explained in SECTION????, and FIGURE ????? The acceleration of the gondola is calculated, The forces acting The following equations 3.5 to 3.7 are the sum of forces acting on the gondola in the coordinate system defined by the plane of the surface of the rear gondola car. As a result most of the forces and reactions acting on the front gondola need to be rotated according to the angle of the hinge, Θ is the angle between the gondolas. Similarly ϕ is the pitch angle of the airship and β is the angle at which the acceleration due to thrust is acting. The reactions are on the left of the equal sign and the known forces acting on the gondola are to the right of the equal sign.

$$\begin{aligned} \Sigma F_x : (m_1 + m_2)a_x + F_{NB3_x} + F_{NB4_x} = \\ \sin(\phi)(m_1 + m_2)g + F_{Drive} + \cos(\Theta)F_{Drive} + \cos(\beta)(m_1 + m_2)a_{Thrust} + \frac{\sqrt{2}}{2}\sin(\Theta)F_{Spring} \end{aligned} \quad (3.5)$$

$$\Sigma F_y : F_{NB1_y} - F_{NB2_y} - F_{NB3_y} + F_{NB4_y} = \frac{\sqrt{2}}{2}F_{Spring} - \frac{\sqrt{2}}{2}F_{Spring} \quad (3.6)$$

$$\Sigma F_z : F_{NB1_z} + F_{NB2_z} + F_{NB3_z} + F_{NB4_z} = \cos(\phi)(m_1 + m_2)g - \frac{\sqrt{2}}{2} \cos(\Theta)F_{Spring} - \frac{\sqrt{2}}{2}F_{Spring} + \sin(\beta)(m_1 + m_2)a_{Thrust} + \sin(\Theta)F_{Drive} \quad (3.7)$$

Force solver ??? is used to solve these equations while making some assumptions based on the reactions. All of the F_{NB} the normal forces between the bearings and the keel. since the contact surface is at 45° between the XY and XZ planes, the magnitudes of the forces acting in the z and y directions must be equal.

$$F_{NB1_z} = -F_{NB1_y} \quad (3.8)$$

$$F_{NB2_z} = F_{NB2_y} \quad (3.9)$$

For the bearings on the front gondola as a result of the angle between gondolas, there will also be a force acting in the x direction such that

$$F_{NB3_x} = -\tan(\Theta)F_{NB3_z} \quad (3.10)$$

$$F_{NB4_x} = -\tan(\Theta)F_{NB4_z} \quad (3.11)$$

$$F_{NB3_y} = -\frac{F_{NB3_z}}{\cos(\Theta)} \quad (3.12)$$

$$F_{NB4_y} = \frac{F_{NB4_z}}{\cos(\Theta)} \quad (3.13)$$

The above equations from 3.8 to 3.13 are all encompassed by the switch case, scenario 2, in the Force Solver Code????.

3.4.6 Bolt Compression Force

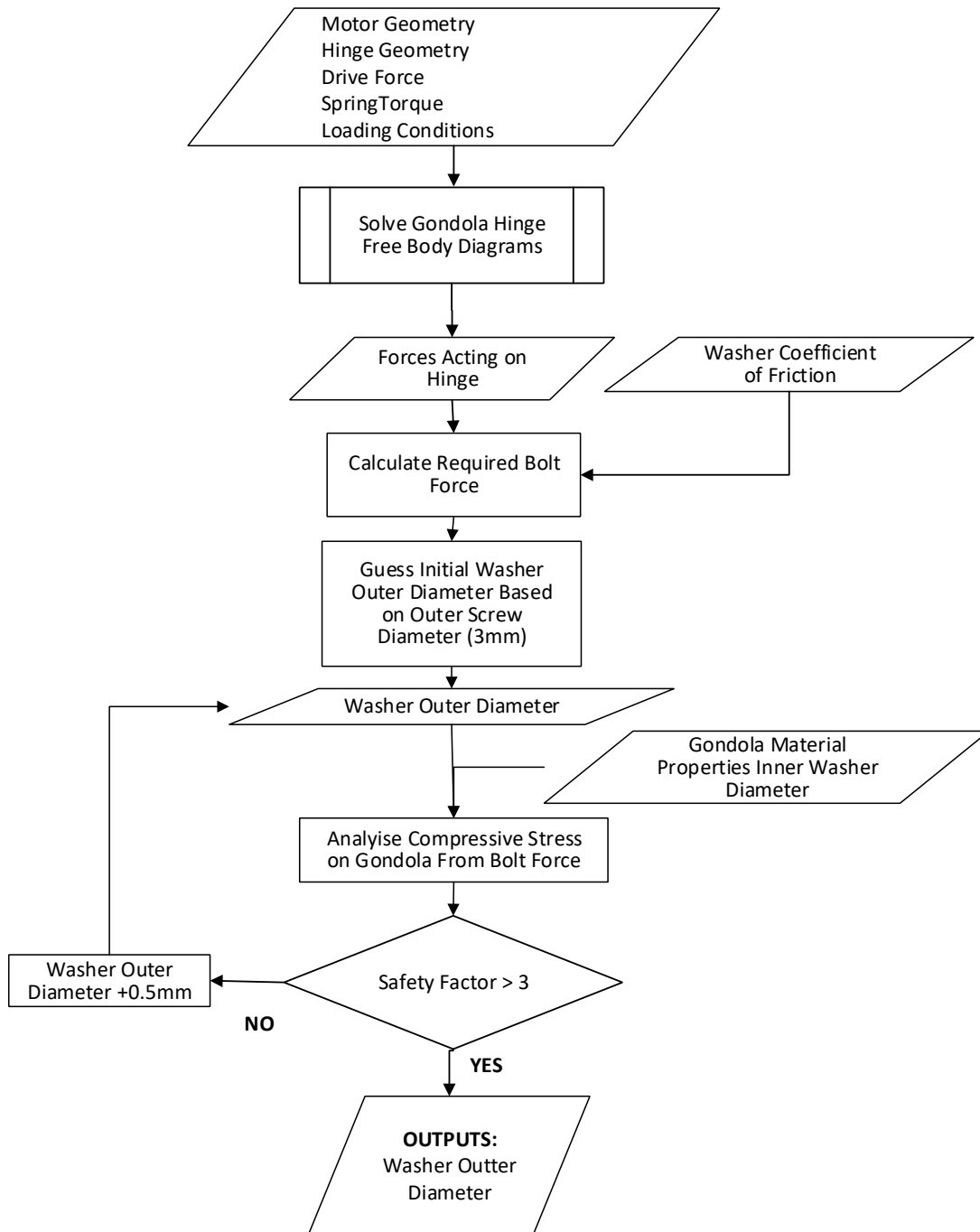


Figure 3.2: Parametrization Outline for the Bolt Compression Force

To fasten the metal hinge to the plastic gondola body, bolts will be used. The reason for this is that they use compression forces to join the two pieces, without requiring threading. Threading a screw into plastic would require female threads in 3D printed plastic, which is inherently bad design and would almost

surely fail.

The main mode of failure for the bolts will not be for the bolt itself, as the forces involved in this design will surely be much less than the yield strength of any potential bolt used. The true concern is the plastic at the interface of the bolt being crushed.

The Bolt compression analysis is meant to ensure that for the Force F_{bolt} , generated by tightening the but and bolt attaching the hinge to the gondola, that the compressive stresses are withstandable by the plastic. The required inputs for the analysis are geometry of the motor and hinge, the positions and size of the bolts used, the spring force from the hinge torsion spring and the drive force calculated from the motor torque. The analysis will output the required outer washer diameter that ensures a safety factor of 3 or greater.

The analysis first computes the bolt tension required to resist the forces parallel to the surface of the hinge. The forces parallel to the bolt are shown in Figure FREEBODY ???. The resultant forces in the XY plane are determined as

$$F_{bshear} = \sqrt{F_{bx'}^2 + F_{by}^2}$$

The only reaction resisting forces in the XY plane will be the friction between the washer and the plastic. It is known that $F_f = \mu NormalForce$. In this case, the normal force is provided by the bolt tension F_{bolt} shown in Figure FREEBODY ???. This bolt tensions must be large enough to generate the required friction force as well as resist the forces acting on it in the z direction. Therefore the required bolt force to ensure no slipping due to shear forces is therefore

$$F_{bolt} = \frac{\sqrt{F_{bx'}^2 + F_{by}^2}}{\mu} + F_{bz} \quad (3.14)$$

μ is estimated as the coefficient of friction between polyethylene and steel, which is 0.2 [6].

Once F_{bolt} is known, the compressive stress of the washer on the plastic gondola body can be determined. This is the critical design factor. If the compressive stress from the washer is too high it will crush the plastic underneath it.

The compressive yield strength ($S_{compressive}$) of Nylon 12 is found to be 6 MPa FIND SOURCE ???. The compressive stress on the gondola by the washer is found to be

$$\sigma_{washer} = \frac{F_{bolt}}{A_{washer}}$$

$$\sigma_{washer} = \frac{F_{bolt}}{\pi(r_o - r_i)^2} \quad (3.15)$$

$$\eta = \frac{S_{compressive}}{\sigma_{washer}} \quad (3.16)$$

If the safety factor is less than 3 the analysis is reiterated with a larger washer outer radius.

3.4.7 Linear Actuator

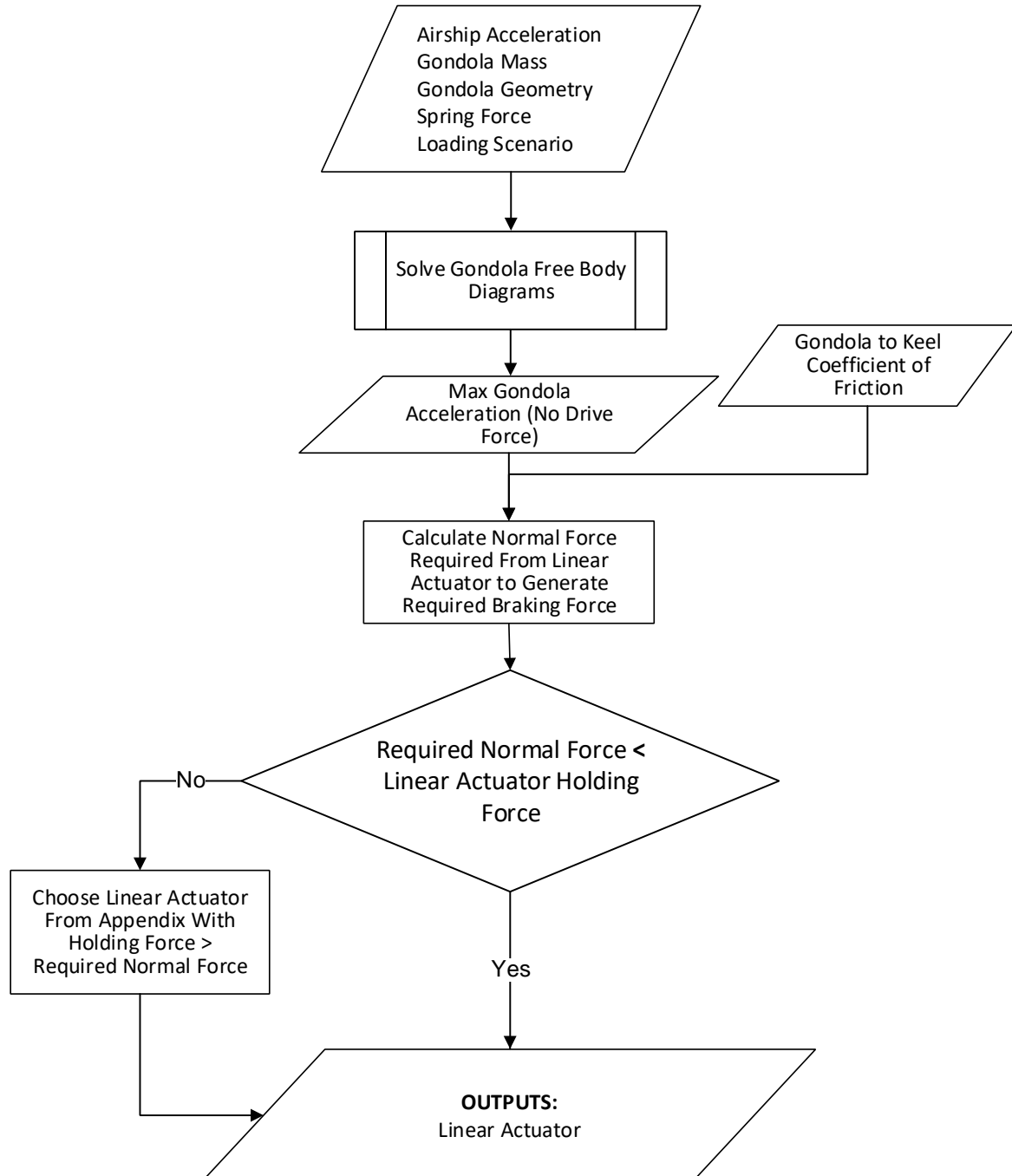


Figure 3.3: Parametrization Outline for the Bolt Compression

The linear actuator analysis is performed to ensure that the holding force of the linear actuator generates a great enough friction to keep the gondola from moving. The analysis first solves for the acceleration

in a scenario similar to that of worst case mention above in REF???? and in friction wheel slip section 3.4.5 with the the friction wheel motor not being powered, therefor the drive force $F_{Drive} = 0$. The inputs required to run this analysis are the geometry of the friction wheel, the motor, the hinge, the gondola, as well as the material properties of the braking surface, the mass of each gondola car, the maximum achievable thruster acceleration and the loading conditions specific to the worst case scenario. The sum of forces used to solve for the case are as follows.

$$\begin{aligned}\Sigma F_x : (m_1 + m_2)a_x + F_{NB3_x} + F_{NB4_x} = \\ \sin(\phi)(m_1 + m_2)g + \cos(\beta)(m_1 + m_2)a_{Thrust} + \frac{\sqrt{2}}{2}\sin(\theta)F_{Spring} \quad (3.17)\end{aligned}$$

$$\Sigma F_y : F_{NB1_y} - F_{NB2_y} - F_{NB3_y} + F_{NB4_y} = \frac{\sqrt{2}}{2}F_{Spring} - \frac{\sqrt{2}}{2}F_{Spring} \quad (3.18)$$

$$\begin{aligned}\Sigma F_z : F_{NB1_z} + F_{NB2_z} + F_{NB3_z} + F_{NB4_z} = \\ \cos(\phi)(m_1 + m_2)g - \frac{\sqrt{2}}{2}\cos(\theta)F_{Spring} - \frac{\sqrt{2}}{2}F_{Spring} + \sin(\beta)(m_1 + m_2)a_{Thrust} \quad (3.19)\end{aligned}$$

The braking force F_{brake} must then be greater than the calculated acceleration a_x . The brake force is dependent on the friction force between the polyurethane and rubber contact piece of the linear actuator, as seen in Figure ????. The breaking force is related to the linear actuator for F_{LA} by the equation 3.20 below.

$$F_{brake} = \mu_{braking surface}F_{LA} \quad (3.20)$$

The value for $\mu_{braking surface}$ is based on the coefficient of friction between rubber and polyurethane which is 0.65 CITESTION???. Once the required linear actuator force is calculated it is compared with the Actuonix linear actuator in Appendix Datasheets D.1 in order to make sure that the force is achievable.

3.4.8 Gondola Arm Stresses

«««; HEAD The failure of the gondola arm will be analysed as shown in Figure 3.4.

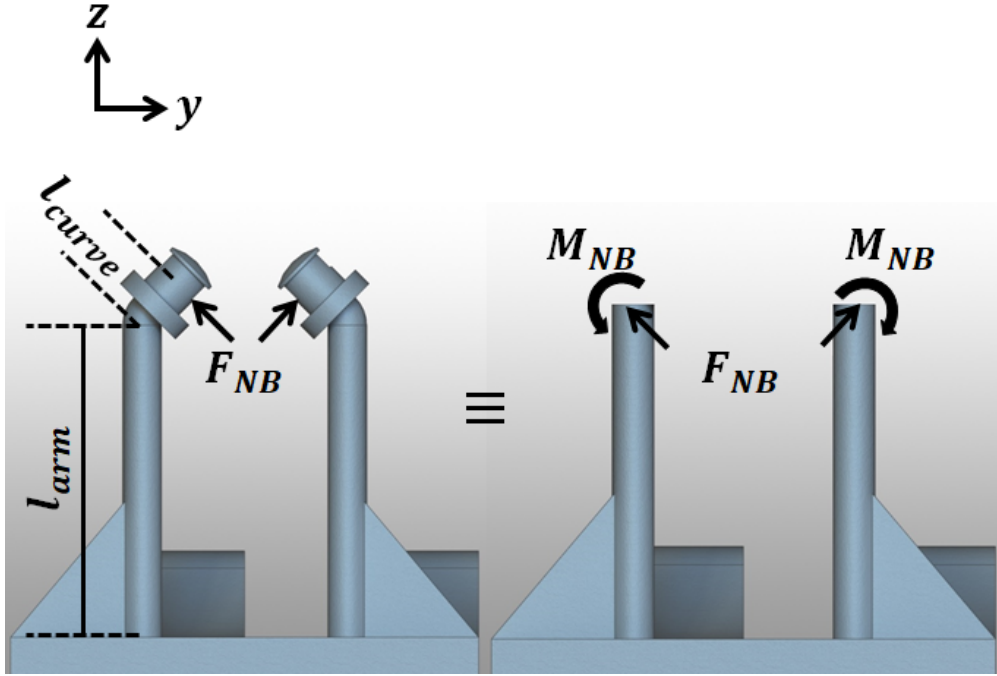


Figure 3.4: Model Used to Compute the Deflection of the Gondola Arms

For the sake of simplicity, the curved section at the very top is ignored and the force is translated from the curved section to the straight section using a force-moment couple. The moment M_{NB} is computed as $M_{NB} = F_{NB}l_{curve}$. Furthermore, the rib seen in Figure 3.4 is ignored. The failure criteria will be computed without the rib, and the rib will be added as an extra preventative measure, to ensure the member is rigid enough.

===== Three analysis were done on the gondola bearing arms. these include deflection, stress concentration analysis and fatigue analysis. However, the only analysis whose results influenced a change in design was the stress concentration. The other two can be found in Appendix sections C.2 and C.3.

The analysis first must solve the gondola forces for the case in which the greatest force is exerted on the bearing arms, when the brake is activated and the airship is thrusting upwards while the pitch remains at 0. This case is explained in REF???. The sum of forces acting on the gondola are.

$$\Sigma F_y : F_{NB1_y} - F_{NB2_y} - F_{NB3_y} + F_{NB4_y} = \frac{\sqrt{2}}{2} F_{Spring} - \frac{\sqrt{2}}{2} F_{Spring} \quad (3.21)$$

$$\begin{aligned} \Sigma F_z : F_{NB1_z} + F_{NB2_z} + F_{NB3_z} + F_{NB4_z} = \\ (m_1 + m_2)g - \frac{\sqrt{2}}{2} F_{Spring} - \frac{\sqrt{2}}{2} F_{Spring} + \sin(\beta)(m_1 + m_2)a_{Thrust} \end{aligned} \quad (3.22)$$

The sum of forces in the x direction are not shown because in this scenario, there are no forces acting

in the x direction although the brake is applied. If there were any forces in the x direction since the brake is activated it would be resisted by the braking force F_{brake} . The arm that is subjected to the highest force is usually located opposite to the friction wheel, but the code REF??? will check all the bearing forces, F_{NB} , and determine which is the largest.

The member is most likely fail at the inner interface with the gondola, marked as shown in FIGURE ???. This is due to the fact that this corner will be in tension. Stress is only relevant acting upon the direction of anticipated rotation, in the x-direction. Stress at the inner corner of the arm is found as: »»»
9c32acc2bce62a7252501e1713478b18750eff97

$$\sigma_{GondolaArm} = \sigma_{axial} + \sigma_{bendingforce} + \sigma_{bendingmoment} \quad (3.23)$$

$$\sigma_{GondolaArm} = \left(\frac{F_{NBz}}{A} \right) \hat{k} + \left(\frac{F_{NB_y} l_{armc}}{I} + \frac{M_{NBC}}{I} \right) \hat{j} \quad (3.24)$$

These stresses are converted to principle stresses (as shown in Appendix C.9). These principle stresses are then used to determine the safety factor by Brittle Mohr-Coulomb Theory [5, 227].

Since $\sigma_a > \sigma_b > 0$,

$$\eta = \frac{S_{ut}}{\sigma_a} \Rightarrow 1.5 \geq \frac{S_{ut}}{\sigma_a} \quad (3.25)$$

3.4.9 Bearing Mounting (Snap-Fit)

The snapfit piece will be subject to a high load when the bearing is being installed, as significant deflection is necessary to allow the bearing into the grooved area. To account for this, there is a gaped section between the arms that allow for deflection. The bearing snap fit will be subject to potential failure at point at the outer edge of the shaft at the bottom of the snap fit cut shown in FIG?????. The analysis determines the minimum required cut depth in order to meet a safety factor of 1.5. The require inputs for this analysis are the bearing shaft diameter, the snap fit overhang and the material properties of nylon 12. These values are both constant as the shaft diameter is based on the inner diameter of the bearing used which will not be changing, this is justified by the analysis done in the Appendix Section C.1. The choice of overhang coincides with the dimensions of the bearing used which can be seen in Appendix Datasheet D.2.

The analysis first computes the the force required for the deflection that must occur for the the snap fit to close to allow the bearing to slide onto the shaft. This calculation is done based on an initially chosen cut depth. The over hang is 1mm so the required deflection of each side of the snap cut is 1mm. The force required to achieve the the 1mm deflection $F_{Snapfit}$ is calculated by modeling the snap fit as a cantilever beam with a concentrated load, cantilevered at the depth of the cut into the shaft $L_{Snapfit}$.

$$F_{Snapfit} = \frac{3\delta EI}{L_{snapfit}^3} \quad (3.26)$$

Because of the geometry each side of the snap fit the distance the moment of inertia was calculated using the following equations REF???. θ in the equation is the angle that forms between the point in the center of the cut edge and the outside of the cut edge as seen in Figure 3.5.

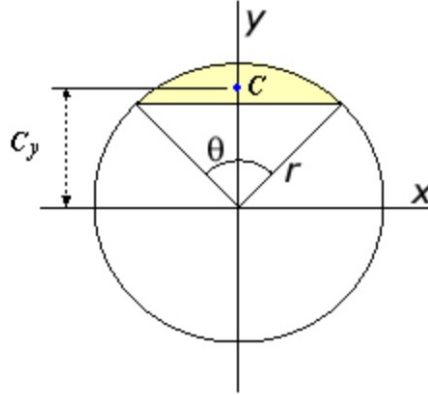


Figure 3.5: Centeroid of Section of Circle [32]

$$I = \left(\frac{r_{Snap}^4}{8} \right) \left(\theta - \sin(\theta) + 2 \sin(\theta) (\sin^2 \left(\frac{\theta}{2} \right)) \right) \quad (3.27)$$

The maximum stress $\sigma_{Snapfit}$ will occur at the outer edge of the shaft at the bottom of the snap fit cut shown in FIG?????, and is calculated using the following equation.

$$\sigma_{Snapfit} = \frac{F_{Snapfit} L_{snapfit} c}{I} \quad (3.28)$$

The distance from the point the force is being applied to the neutral axis c in equation 3.28, is calculated by computing the length C_y from Figure ?? and subtracting it from the shaft radius plus the snap fit overhang. This can be seen in equation 3.29.

$$c = r_{overhang} - \frac{4r_{Snap}}{3} \left(\frac{\sin^3 \left(\frac{\theta}{2} \right)}{\theta - \sin(\theta)} \right) \quad (3.29)$$

This safety factor is slightly lower than other analysis with high failure likelihood which can be found in table 3.1. This is due to the fact that the installation will only be performed once. Maximum stress under normal loading conditions will be a direct result of the normal force applied on the bearing by the keel.

Chapter 4: Discussion

Discussion and Critical Review of Design aka Talk shit about ourselves

Bibliography

- [1] Actuonix Motion Devices. Miniature Linear Motion Series - L12, 2016. URL <https://s3.amazonaws.com/actuonix/Actuonix+L12+Datasheet.pdf>.
- [2] Advanced Mechanical Engineering Solutions. Metric Bolt Grades Strength, 2017. URL <http://www.amesweb.info/Screws/Metric\Bolt\Grades\Strength.aspx>.
- [3] Hoda Amel. *Investigating the Cyclic Performance of Laser Sintered Nylon 12*. PhD thesis, University of Sheffield, 2015. URL <http://etheses.whiterose.ac.uk/11927/1/Investigating the Cyclic Performance of Laser Sintered Nylon 12-Hoda Amel-110203386.pdf>.
- [4] Steven A. Brandt and American Institute of Aeronautics and Astronautics. *Introduction to aerodynamics : a design perspective*. American Institute of Aeronautics and Astronautics, 2004. ISBN 9781563477010.
- [5] Budynas and Nisbett. Shigley's Mechanical Engineering Design, Eighth Edition. *Analysis*, page 1059, 2006. ISSN 0717-6163. doi: 10.1007/s13398-014-0173-7.2.
- [6] Engineers Edge. Coefficients of Friction. URL <https://www.engineersedge.com/coeffients\of\friction.htm>.
- [7] Szabolcs Füzesi. Static Thrust Calculator - STRC, 2017. URL <http://www.godolloairport.hu/calc/strc\eng/index.htm>.
- [8] HobbyKing. Rhino 2250mAh 3S 11.1v 40C Lipoly Pack, . URL https://hobbyking.com/en\us/rhino-2250mah-3s-11-1v-40c-lipoly-pack.html?{_\}\{_\}\{_\}store=en\us.
- [9] HobbyKing. TURNIGY Plush 10amp Speed Controller w/BEC, . URL <https://hobbyking.com/en\us/turnigy-plush-10amp-9gram-speed-controller.html>.
- [10] HobbyKing. Turnigy 20A BRUSHED ESC, . URL https://hobbyking.com/en\us/turnigy-20a-brushed-esc.html?{_\}\{_\}\{_\}store=en\us.
- [11] HobbyKing. PixFalcon Micro PX4 Autopilot, . URL <https://hobbyking.com/en\us/pixfalcon-micro-px4-autopilot.html>.
- [12] HobbyKing. UBLOX Micro M8N GPS Compass Module (1pc), . URL <https://hobbyking.com/en\us/ublox-micro-m8n-gps-compass-module-1pc.html>.
- [13] HobbyKing. Aerostar Carbon Fibre Propeller 7x5, . URL https://hobbyking.com/en\us/aerostar-carbon-fibre-propeller-7x5-1pcs.html?{_\}\{_\}\{_\}store=en\us.
- [14] HobbyKing. FrSky TFR6M 2.4Ghz 6CH Micro Receiver FASST Compatible, . URL <https://hobbyking.com/en\us/frsky-tfr6m-2-4ghz-6ch-micro-receiver-fasst-compatible.html>.

- [15] HobbyKing. HobbyKing® TM 2612 Brushless Outrunner 1900KV, . URL https://hobbyking.com/en{_}us/hobbykingr-tm-2612-brushless-outrunner-1900kv.html?gclid=CjwKCAjwgvf0BRB7EiwAeP7ehmx-1gQwKEcajtpPc1NNf0p82N1T2DdM6I-PFOINiIxTERGAn2ZBdhoCJIQQAvD{_}BwE{_}gclsrc=aw.ds.
- [16] HobbyKing. Micro HKPilot Telemetry radio Set With Integrated PCB Antenna 915Mhz, . URL https://hobbyking.com/en{_}us/micro-hkpilot-telemetry-radio-set-with-integrated-pcb-antenna-915mhz.html.
- [17] Lapp Group. SKINTOP ST-M Data Sheet, 2017. URL https://products.lappgroup.com/fileadmin/documents/technische{_}doku/datenblaetter/skintop/DB53111000EN.pdf.
- [18] MatWeb. Overview of materials for Epoxy/Carbon Fiber Composite, 2017. URL http://www.matweb.com/search/DataSheet.aspx?MatGUID=39e40851fc164b6c9bda29d798bf3726{_}ckck=1.
- [19] McMaster-Carr. McMaster-Carr - Neoprene Roller, Drive, Aluminum Hub, 5/8" Roller Diameter, 3/16" Roller Width, . URL https://www.mcmaster.com/{\#}60885k31/_19r8ni4.
- [20] McMaster-Carr. McMaster-Carr - General Purpose Plastic Ball Bearing, with Stainless Steel Ball, for 1/4" Shaft Diameter, 5/8" OD, . URL https://www.mcmaster.com/{\#}6455k2/_19nl4h4.
- [21] McMaster-Carr. McMaster-Carr - Alloy Steel Cup-Point Set Screw, Black Oxide, 8-32 Thread, 1/4" Long, . URL https://www.mcmaster.com/{\#}91375a190/_19r8q0o.
- [22] McMaster-Carr. McMaster-Carr - Music-Wire Steel Torsion Spring, 180 Degree Right-Hand Wound, 0.767" OD, . URL https://www.mcmaster.com/{\#}9271k271/_19r8qyv.
- [23] Michigan Technological University. Properties of Selected Matrices, 2017. URL <http://www.mse.mtu.edu/{\sim}drjohn/my4150/props.html>.
- [24] Pololu. 50:1 Micro Metal Gearmotor HP 6V, . URL <https://www.pololu.com/product/998/specs>.
- [25] Pololu. Magnetic Encoder Pair Kit for Micro Metal Gearmotors, 12 CPR, 2.7-18V (HPCB compatible), . URL <https://www.pololu.com/product/3081/pictures>.
- [26] RobotShop. HS-7950TH Ultra Torque HV Coreless Titanium Gear Servo - RobotShop. URL http://www.robotshop.com/ca/en/hs-7950th-ultra-torque-coreless-titanium-gear-servo.html?gclid=CjwKCAjwgvf0BRB7EiwAeP7ehmVw7Ku4Ih2HYJeFV34wtpf0lmQIOCX5BXYQ00f48oI4lGOzHuABnRoCKiEQAvD{_}BwE.
- [27] Servo City. HS-7950TH Servo, 2017. URL <https://www.servocity.com/hs-7950th-servo>.

- [28] Gabriel Staples. Propeller Static & Dynamic Thrust Calculation - Part 1 of 2, 2013. URL <http://www.electricrcaircraftguy.com/2013/09/propeller-static-dynamic-thrust-equation.html>.
- [29] Gabriel Staples. Propeller Static & Dynamic Thrust Calculation - Part 2 of 2, 2015. URL <http://www.electricrcaircraftguy.com/2014/04/propeller-static-dynamic-thrust-equation-background.html>.
- [30] War Department. Technical Manual of Airship Aerodynamics. Technical report, Washington, 1941. URL https://www.faa.gov/regulations__policies/handbooks__manuals/aviation/media/airship__aerodynamics.pdf.
- [31] Wikipedia. Cauchy Stress Tensor, 2017. URL https://en.wikipedia.org/wiki/Cauchy__stress__tensor.
- [32] Wolfram. Engineering Fundamentals: CENTROID, AREA, MOMENTS OF INERTIA, POLAR MOMENTS OF INERTIA, & RADIUS OF GYRATION OF A CIRCLE. URL <http://www.efunda.com/math/areas/CircularSegment.cfm>.

Appendix A: Instructions for Installing and Running the GUI

yep

Appendix B: Code

B.1 Code 1

```
1 function lab1
2
3 disp('_____');
4 disp('_____');
5 disp('| Lab 1 |');
6 disp('_____');
7 disp('_____');
8
9
10 % Point we are using as x_i
11 x = 5.0;
12
13 % Delta x's that we will use in our finite-difference approximations
14 dx1 = 0.5;
15 dx2 = dx1/2;
16 dx3 = dx2/2;
17 dx4 = dx3/2;
18 dx5 = dx4/2;
19
20 % Exact derivative of y at x=5
21 exact1 = dy(5.0);
22
23 %%%%%%
24 % Approximation of the first derivative
25
26 approx11 = dyapprox(x, dx1);
27 approx12 = dyapprox(x, dx2);
28 approx13 = dyapprox(x, dx3);
29 approx14 = dyapprox(x, dx4);
30 approx15 = dyapprox(x, dx5);
31
32 % Errors using first-order method
33 disp('Errors for first-order finite-difference , (first column of table)')
34 error11 = abs(exact1 - approx11)
35 error12 = abs(exact1 - approx12)
36 error13 = abs(exact1 - approx13)
37 error14 = abs(exact1 - approx14)
38 error15 = abs(exact1 - approx15)
```

```

40 % Order of convergence
41 disp('Actual order of convergence for first-order method, (second column of table)')
42 order11 = log(error12/error11)/log(dx2/dx1)
43 order12 = log(error13/error12)/log(dx3/dx2)
44 order13 = log(error14/error13)/log(dx4/dx3)
45 order14 = log(error15/error14)/log(dx5/dx4)
46
47%%%%%%%%%%%%%
48 % Approximation of the second derivative
49
50 %Exact second derivative of y at x=5
51 exact2 = d2y(5.0);
52
53 approx21 = d2yapprox(x, dx1);
54 approx22 = d2yapprox(x, dx2);
55 approx23 = d2yapprox(x, dx3);
56 approx24 = d2yapprox(x, dx4);
57 approx25 = d2yapprox(x, dx5);
58
59 % Errors using first-order method
60 disp('Errors for first-order finite-difference, (first column of table)')
61 error21 = abs(exact2 -approx21)
62 error22 = abs(exact2 -approx22)
63 error23 = abs(exact2 -approx23)
64 error24 = abs(exact2 -approx24)
65 error25 = abs(exact2 -approx25)
66
67 % Order of convergence
68 disp('Actual order of convergence for first-order method, (second column of table)')
69 order21 = log(error22/error21)/log(dx2/dx1)
70 order22 = log(error23/error22)/log(dx3/dx2)
71 order23 = log(error24/error23)/log(dx4/dx3)
72 order24 = log(error25/error24)/log(dx5/dx4)
73
74%%%%%%%%%%%%%
75 % Approximation of the third derivative
76
77 %Exact third derivative of y at x=5
78 exact3 = d3y(5.0);
79
80 approx31 = d3yapprox(x, dx1);
81 approx32 = d3yapprox(x, dx2);
82 approx33 = d3yapprox(x, dx3);
83 approx34 = d3yapprox(x, dx4);
84 approx35 = d3yapprox(x, dx5);

```

```

85
86 % Errors using first-order method
87 disp('Errors for first-order finite-difference, (first column of table)')
88 error31 = abs(exact3 -approx31)
89 error32 = abs(exact3 -approx32)
90 error33 = abs(exact3 -approx33)
91 error34 = abs(exact3 -approx34)
92 error35 = abs(exact3 -approx35)
93
94 % Order of convergence
95 disp('Actual order of convergence for first-order method, (second column of table)')
96 order31 = log(error32/error31)/log(dx2/dx1)
97 order32 = log(error33/error32)/log(dx3/dx2)
98 order33 = log(error34/error33)/log(dx4/dx3)
99 order34 = log(error35/error34)/log(dx5/dx4)
100
101%%%%%%%%%%%%%
102%%%%%%%%%%%%%
103% Produce plots
104%%%%%%%%%%%%%
105%%%%%%%%%%%%%
106
107% Number of points in the plots
108% - Adjust this to adjust how small Delta x gets.
109% It starts at 1/2 and is divided by 2 "n" times
110 n = 33;
111
112% Initialize Storage
113 dxs = zeros(n,1);
114 errors1 = zeros(n,1);
115 errors2 = zeros(n,1);
116 errors3 = zeros(n,1);
117
118% loop through, filling "d_xs", "errors1", "errors2", and "errors3".
119 for i = 1:n
120 % Each time through the loop, Delta x is half as big
121 d_xs(i) = 0.5^i;
122 errors1(i)=abs(exact1-dyapprox(x,d_xs(i)));
123 errors2(i)=abs(exact2-d2yapprox(x,d_xs(i)));
124 errors3(i)=abs(exact3-d3yapprox(x,d_xs(i)));
125 end
126
127% Compute the log of the inverse of delta x
128 loginvdxs = log10(1./d_xs);
129

```

```

130 % Compute the log of the errors
131 logerrors1 = log10(errors1);
132 logerrors2 = log10(errors2);
133 logerrors3 = log10(errors3);
134
135 % Compute reference lines with the expected slope
136 % - the "-2" is just an offset so that the reference
137 % line does not intersect the error line.
138 reffline1 = -3*loginvdxs -2;
139 reffline2 = -2*loginvdxs -2;
140 reffline3 = -1*loginvdxs -2;
141
142 %%%%%%
143 % Make three figures
144 figure(1);
145 plot(loginvdxs,logerrors1,'-o',loginvdxs,reffline1)
146 legend('finite-difference','reference', 'slope = -3')
147 title('Third-order finite-difference error for the first derivative as a function of Delta x')
148 xlabel('log10(1/Delta x)')
149 ylabel('log10(error)')
150
151 figure(2);
152 plot(loginvdxs,logerrors2,'-o',loginvdxs,reffline2)
153 legend('finite-difference','reference', 'slope = -2')
154 title('Second-order finite-difference error for the second derivative as a function of Delta x')
155 xlabel('log10(1/Delta x)')
156 ylabel('log10(error)')
157
158 figure(3);
159 plot(loginvdxs,logerrors3,'-o',loginvdxs,reffline3)
160 legend('finite-difference','reference', 'slope = -1')
161 title('First-order finite-difference error for the third derivative as a function of Delta x')
162 xlabel('log10(1/Delta x)')
163 ylabel('log10(error)')
164
165 end
166
167
168 %%%%%%
169 % The function we are analysing evaluated at x
170 %%%%%%
171 function output = y(x)

```

```

172     output = (x^3)*sin(x);
173 end
174
175 %%%%%%%%%%%%%%%%%%%%%%%%%%%%%%%%%%%%%%
176 % The exact derivative of the function we are analysing
177 % evaluated at x.
178 %%%%%%%%%%%%%%%%%%%%%%%%%%%%%%%%%%%%%%
179 function output = dy(x)
180     output = 3*x^2*sin(x)+x^3*cos(x);
181 end
182
183 %%%%%%%%%%%%%%%%%%%%%%%%%%%%%%%%%%%%%%
184 % The exact second derivative of the function we are analysing
185 % evaluated at x.
186 %%%%%%%%%%%%%%%%%%%%%%%%%%%%%%%%%%%%%%
187 function output = d2y(x)
188     output = 6*x^2*cos(x)+(6*x-x^3)*sin(x);
189 end
190
191 %%%%%%%%%%%%%%%%%%%%%%%%%%%%%%%%%%%%%%
192 % The exact third derivative of the function we are analysing
193 % evaluated at x.
194 %%%%%%%%%%%%%%%%%%%%%%%%%%%%%%%%%%%%%%
195 function output = d3y(x)
196     output = (18*x-x^3)*cos(x)+(6-9*x^2)*sin(x);
197 end
198
199 %%%%%%%%%%%%%%%%%%%%%%%%%%%%%%%%%%%%%%
200 % A third-order approximation to the derivative of y
201 % at x using a step size of "dx"
202 %%%%%%%%%%%%%%%%%%%%%%%%%%%%%%%%%%%%%%
203 function output = dyapprox(x,dx)
204     output = (1.0/(6*dx))*(-11*y(x)+18*y(x+dx)-9*y(x+2*dx)+2*y(x+3*dx));
205 end
206
207 %%%%%%%%%%%%%%%%%%%%%%%%%%%%%%%%%%%%%%
208 % A second-order approximation to the second derivative of y
209 % at x using a step size of "dx"
210 %%%%%%%%%%%%%%%%%%%%%%%%%%%%%%%%%%%%%%
211 function output = d2yapprox(x,dx)
212     output = 1.0/(dx*dx)*(2*y(x)-5*y(x+dx)+4*y(x+2*dx)-y(x+3*dx));
213 end
214
215 %%%%%%%%%%%%%%%%%%%%%%%%%%%%%%%%%%%%%%
216 % A first-order approximation to the third derivative of y

```

```
217 % at x using a step size of "dx"
218 %%%
219 function output = d3yapprox(x,dx)
220     output = 1.0/(dx*dx*dx)*(-1*y(x)+3*y(x+dx)-3*y(x+2*dx)+y(x+3*dx));
221 end
```

Appendix C: Additional Material

C.1 Gondola Bearings

Test

C.2 Gondola Arm Deflection

To ensure that the gondola will not fall off of the keel during operation, a deflection calculation is computed on the gondola arm. The maximum deflection of the gondola arm is modelled in a similar fashion to the Gondola Arm Stress Analysis in Section 3.4.8.

The deflection will be calculated using simple beam equations. The force F_{NB} is resolved into y and z components. The deflection is then computed in three separate parts, as shown below:

$$\delta_{GondolaArm} = \delta_{axial} + \delta_{bendingforce} + \delta_{bendingmoment} \quad (C.1)$$

$$\delta_{GondolaArm} = \left(\frac{F_{NB_z} l_{arm}}{AE} \right) \hat{k} + \left(\frac{F_{NB_y} l_{arm}^3}{3EI} + \frac{M_{NB} l_{arm}^2}{2EI} \right) \hat{j} \quad (C.2)$$

The failure possibility here would be for the arm to deflect enough that the gondola falls off the keel. This occurs when the total deflection δ is larger than $0.5cm$, which is half of the width of the keel face. Since both arms can deflect at the same time, they can be combined to reach $0.5cm$. Therefore it is required that the result of Equation C.2 be less than $0.25cm$. Therefore the equation to optimize is:

$$0.25 \leq \sqrt{\left(\frac{F_{NB_z} l_{arm}}{AE} \right)^2 + \left(\frac{F_{NB_y} l_{arm}^3}{3EI} + \frac{M_{NB} l_{arm}^2}{2EI} \right)^2} \quad (C.3)$$

C.3 Gondola Arm Fatigue Failure

The loading and unloading of the plastic gondola arm due to the reaction force of the keel on the gondola motor could potentially cause a fatigue failure. A paper on cyclic performance of Laser Sintered Nylon [3] was used to quantify the effects of fatigue on the plastic. Very little research has been done for fatigue failure of 3D printed material. The laser sintering process is similar to 3D printing in that it melts layers of plastic in succession to obtain complex geometries with no pre-existing tooling required. Because of this, the laser sintering process creates shear planes, much like those created in 3D printing. For this reason, the paper was as a basis for the fatigue analysis of the 3D printed part, as these shear planes are critical to the fatigue strength of the material.

The S-N curve shown in Figure C.1 was used to determine the maximum nominal stress that the gondola could take, thus defining the criteria for failure.

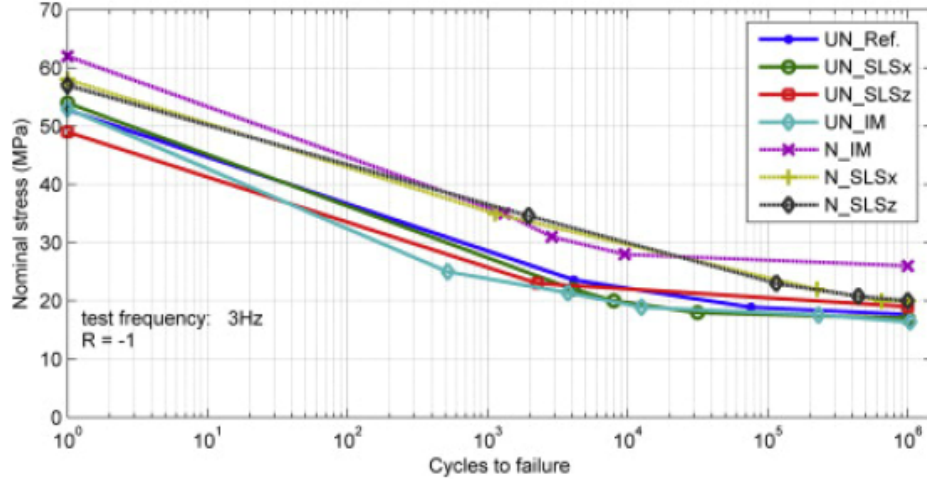


Figure C.1: S-N Curve for Laser Sintered Nylon [3], Used to Determine the Fatigue Failure of the Gondola Body

Assuming that the loading frequency is not higher than around 3hz, no appreciable heat is generated and thus the loading frequency should not affect the cycles to failure. Assuming SLS nylon, the maximum nominal stress for infinite life (10^6 cycles) is $17MPa$. Any higher and the part will fail after enough loading cycles.

To find the nominal stress, the amount of stress fluctuation which the gondola arm will sustain needs to be computed. For this, the lowest stress will be when the gondola is not moving, and is only loaded by the weight of the gondola itself. The highest stress will be when the gondola motor is on at full force, at the worst case scenario **DESCRIBED HERE** bending the gondola arm. These both conditions are computed using **ISAAKS SHIT HERE**, and two values of F_{NB} are found. The difference between the two is the fluctuation of stress.

$$\sigma_{worst} = \underbrace{\left[\left(\frac{F_{NB_z}}{A} \right) \hat{k} + \left(\frac{F_{NB_y} l_{arm} c}{I} + \frac{M_{NB} c}{I} \right) \hat{j} \right]}_{\text{Worst Case } F_{NB}}, \quad \sigma_{best} = \underbrace{\left[\left(\frac{F_{NB_z}}{A} \right) \hat{k} + \left(\frac{F_{NB_y} l_{arm} c}{I} + \frac{M_{NB} c}{I} \right) \hat{j} \right]}_{\text{Best Case } F_{NB}} \quad (C.4)$$

The principle stress for each case σ_a is found, and the difference is computed to get the nominal strength, which must be less than $17MPa$. Therefore the optimized equation is:

$$17Mpa \geq |\sigma_{best} - \sigma_{worst}| \quad (C.5)$$

C.4 Thruster Motor

C.5 Thruster Arm Adhesion

To connect the carbon fibre arm to the aluminium body which holds the thruster assembly, epoxy will be used. The carbon fibre arm will slide into an aluminium pocket welded to the aluminium thruster plate, as shown in Figure **ADD RENDERED FIGURE HERE**.

The analysis will be conducted by assuming the adhesion surface will be like a double lap joint, shown in Figure C.2 below.

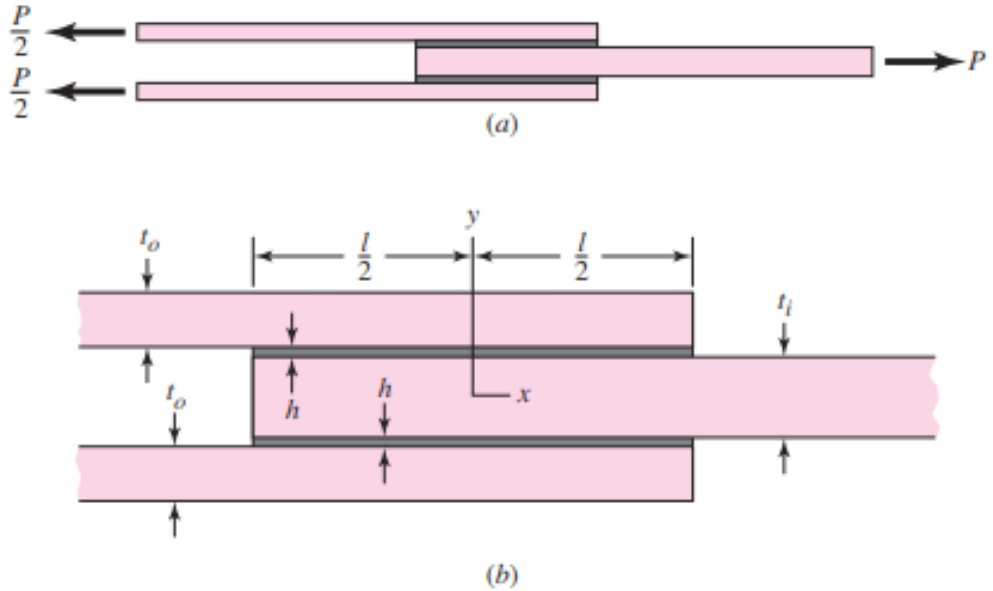


Figure C.2: Analysis of Carbon Fibre Adhesion (From Shigley's Machine Design [5, 484])

The shear-stress distribution of the joint is given by

$$\tau(x) = \frac{P\omega}{4bsinh(\omega l/2)}cosh(\omega x) + \left[\frac{P\omega}{4bcosh(\omega l/2)} \left(\frac{2E_0t_0 - E_it_i}{2E_0t_0 + E_it_i} \right) + \frac{(\alpha_i - \alpha_0)\Delta T\omega}{(1/E_0t_0 + 2/E_it_i)cosh(\omega l/2)} \right] sinh(\omega x) \quad (C.6)$$

$$\omega = \sqrt{\frac{G}{h} \left(\frac{1}{E_0t_0} + \frac{2}{E_it_i} \right)} \quad (C.7)$$

Where E_o , t_0 α_0 and E_i , t_i α_i are the modulus, thickness, coefficient of thermal expansion for the outer and inner adherend, respectively. G , h , b and l are the shear modulus, thickness, width and length of the adhesive, respectively. ΔT is the change in temperature of the joint, from its curing temperature (zero stress temperature). The closer the curing temperature of the adhesive is to the operating temperature, the

lower the thermal stresses induced in the joint will be.

For this case, an unmodified epoxy will be selected as the adhesive material. From [5], Table 9-7, the lap-shear strength can be anywhere from $10.3 - 27.6 \text{ MPa}$. 10.3 MPa will be selected as a conservative estimate.

The outer material is aluminium and the inner material will be carbon fibre. Because of the nature of aluminium, an extremely thin layer of fibreglass should be added between the carbon fibre and aluminium to prevent corrosion due to the curing of the epoxy. Data was found as follows:

$$\begin{aligned} G &= 1.3 \text{ GPa} [23] \\ E_i &= 109 \text{ GPa} [18] \\ \alpha_i &= 23.7 * 10^{-6} \text{ mm/mm}^\circ\text{C} [18] \\ E_0 &= 71 \text{ GPa} [5] \\ \alpha_0 &= 23.94 \text{ mm/mm}^\circ\text{C} [5] \end{aligned}$$

ΔT can be estimated by assuming the epoxy is cured at room temperature (20°C) and that the lowest temperature the blimp will be used at is -40°C . This yields $\Delta T = -60^\circ\text{C}$. The thickness of the adhesive will be estimated as $h = 0.5 \text{ mm}$. As preliminary estimates, $t_0 = 9.73 \text{ mm}$, $t_i = 9.73 \text{ mm}$, $l = 30 \text{ mm}$, and $b = 50.80 \text{ mm}$. The force P can be estimated using **SOME STUFF** $P = 100 \text{ N}$.

Substituting these values into Equation C.7 yields

$$\omega = \sqrt{\frac{1300 \text{ MPa}}{0.5 \text{ mm}} \left(\frac{1}{71000 \text{ MPa} * 9.73 \text{ mm}} + \frac{2}{109000 \text{ MPa} * 9.73 \text{ mm}} \right)} = 0.0930946 \text{ mm}^{-1} \quad (\text{C.8})$$

Followed by substitution into Equation C.6:

$$\begin{aligned} \tau(x) &= \frac{100 \text{ N} * 0.0930946 \text{ mm}^{-1}}{4 * 50.80 \text{ mm} * \sinh(0.0930946 \text{ mm}^{-1} * 30 \text{ mm}/2)} \cosh(0.0930946 \text{ mm}^{-1} * x) + \\ &\quad \left[\frac{100 \text{ N} * 0.0930946 \text{ mm}^{-1}}{4 * 50.80 \text{ mm} * \cosh(0.0930946 \text{ mm}^{-1} * 30 \text{ mm}/2)} \left(\frac{2 * 71000 \text{ MPa} * 9.73 \text{ mm} - 1300 \text{ MPa} * 9.73 \text{ mm}}{2 * 71000 \text{ MPa} * 9.73 \text{ mm} + 1300 \text{ MPa} * 9.73 \text{ mm}} \right) + \right. \\ &\quad \left. \frac{(23.7 * 10^{-6} \text{ mm/mm}^\circ\text{C} - 23.94 * 10^{-6} \text{ mm/mm}^\circ\text{C}) * (-60^\circ\text{C}) * 0.0930946 \text{ mm}^{-1}}{\left(\frac{1}{71000 \text{ MPa} * 9.73 \text{ mm}} + \frac{2}{109000 \text{ MPa} * 9.73 \text{ mm}} \right) \cosh(0.0930946 \text{ mm}^{-1} * 30 \text{ mm}/2)} \right] \sinh(0.0930946 \text{ mm}^{-1} * x) \\ &= 0.02416 \text{ MPa} * \cosh(0.0930946 \text{ mm}^{-1} * x) + [0.02098 \text{ MPa} + 0.1871 \text{ MPa}] \sinh(0.0930946 \text{ mm}^{-1} * x) \end{aligned} \quad (\text{C.9})$$

at $x = l/2 = 30 \text{ mm}/2$, the shear is at a maximum value. Therefore, the shear force is $\tau = 0.4464 \text{ MPa}$, Yielding a safety factor of $\eta = 10.3 \text{ MPa}/0.4464 \text{ MPa} = 23.0734$.

C.6 Thruster Bearings

C.7 Gondola Motor Shaft

C.8 Vectoring Shaft Screw Axial Loading Conditions

The screw which secures the nylon vectoring shaft is part of the servo motor assembly. The servo motor output is a spline with a female thread for a 3mm screw to be threaded into (Servo example from ServoCity [27]), as shown in Figure C.3.



Figure C.3: HS-7950TH Servo Spline Attachment [27]

One potential concern would be for the small 3mm screw (which threads into the spline) breaking if an axial load was applied to it. While there is *theoretically* no scenario where any axial load is applied, it is worth checking the strength of the screw, because during transportation of the airship it is possible that the part may be unintentionally pulled. To find the proof force of the bolt, it was assumed that the bolt was a SAE Class 4.8 M3-0.5, and the following properties were found:

Table C.1: Table of Bolt Strength for a M3-0.5 Bolt [2]

RESULTS			
Parameter	Symbol	Value	Unit
Designation	--	M3x0.5	
Property Class	-	4.8	---
Screw Thread Series	--	Coarse	
Nominal Stress Area	A_{s_nom}	5.03	mm^2
Minimum Tensile Strength	R_m_{min}	420	MPa
Minimum Ultimate Tensile Load	-	2110	N
Minimum Stress at 0,2 % non-proportional elongation	$R_{p0.2}_{min}$	---	MPa
Stress Under Proof Load	s_p	310	
Proof Load	-	1560	N
Minimum Breaking Torque	M_B_{min}	---	N.m
Vickers Hardness , $F \geq 98 \text{ N}$	Minimum	130	HV
	Maximum	220	
Minimum Brinell Hardness , $F = 30 \text{ D}^2$	Minimum	124	HBW
	Maximum	209	

Based on this, the tensile load of the bolt is 2110N, which is much higher than any axial forces that the shaft is expected to have to withstand. Therefore the design is not a problem.

C.9 Cauchy Stress Tensor [31]

The Cauchy Stress tensor fully defines the stresses acting on an infinitesimally small element within a material. It is particularly useful for failure analysis, as it is the internal stresses within a material that are

used to determine the safety factor of the material at a specific location. Its general forms are shown below.

$$\sigma = \begin{bmatrix} \sigma_{11} & \sigma_{12} & \sigma_{13} \\ \sigma_{21} & \sigma_{22} & \sigma_{23} \\ \sigma_{31} & \sigma_{32} & \sigma_{33} \end{bmatrix} \equiv \begin{bmatrix} \sigma_{xx} & \sigma_{xy} & \sigma_{xz} \\ \sigma_{yx} & \sigma_{yy} & \sigma_{yz} \\ \sigma_{zx} & \sigma_{zy} & \sigma_{zz} \end{bmatrix} \equiv \begin{bmatrix} \sigma_x & \tau_{xy} & \tau_{xz} \\ \tau_{yx} & \sigma_y & \tau_{yz} \\ \tau_{zx} & \tau_{zy} & \sigma_z \end{bmatrix} \quad (\text{C.10})$$

Generally, the use of failure theories requires knowing the *principal stresses*. These are located perpendicular to the *principal planes*. Any body in a state of stress will have three principal planes, where there are no normal shear stresses, only three *principal stresses*.

Any stress tensor can undergo a change of coordinates to obtain the principal stresses. The transformed stress tensor can be written as follows:

$$\sigma' = \begin{bmatrix} \sigma_1 & 0 & 0 \\ 0 & \sigma_2 & 0 \\ 0 & 0 & \sigma_3 \end{bmatrix} \quad (\text{C.11})$$

Obtaining the principle stresses is relatively simple. The principle stresses are simply the eigenvalues of the stress tensor. MATLAB is used to find the eigenvalues of a given stress tensor, and the principle stresses are given by

$$\sigma_1 = \max(\lambda_1, \lambda_2, \lambda_3) \quad (\text{C.12})$$

$$\sigma_3 = \min(\lambda_1, \lambda_2, \lambda_3) \quad (\text{C.13})$$

$$\sigma_2 = \sigma_{11} + \sigma_{22} + \sigma_{33} - \sigma_1 - \sigma_3 \quad (\text{C.14})$$

The principal stresses are then used to conduct failure analysis using the preferred failure analysis method (e.g. Von Mises).

C.10 Previous Drag Analysis

Before knowing that the airship envelope needed to be parametrizable, drag values were initially computed using SolidWorks, by its built in Flow Simulation add-on. Simulations were conducted from 2m/s to 20m/s, at intervals of 2m/s. Skin Friction Drag and Regular Drag were computed and summed to obtain total drag for each speed. A table with the results from the simulations can be seen in Table C.2.

Table C.2: Raw Data From SolidWorks Flow Simulation

Airspeed (m/s)	Drag Force (N)	Skin Friction Force (N)	Total Drag (N)
2	0.4012	0.0651	0.4663
4	1.5286	0.2035	1.7320
6	3.1225	0.4011	3.5236
8	5.2179	0.7063	5.9242
10	8.2517	1.1397	9.3913
12	12.4647	2.0588	14.5235
14	17.4157	3.9501	21.3659
16	22.8193	5.3402	28.1595
18	29.0603	6.8692	35.9296
20	35.6981	8.4702	44.1682

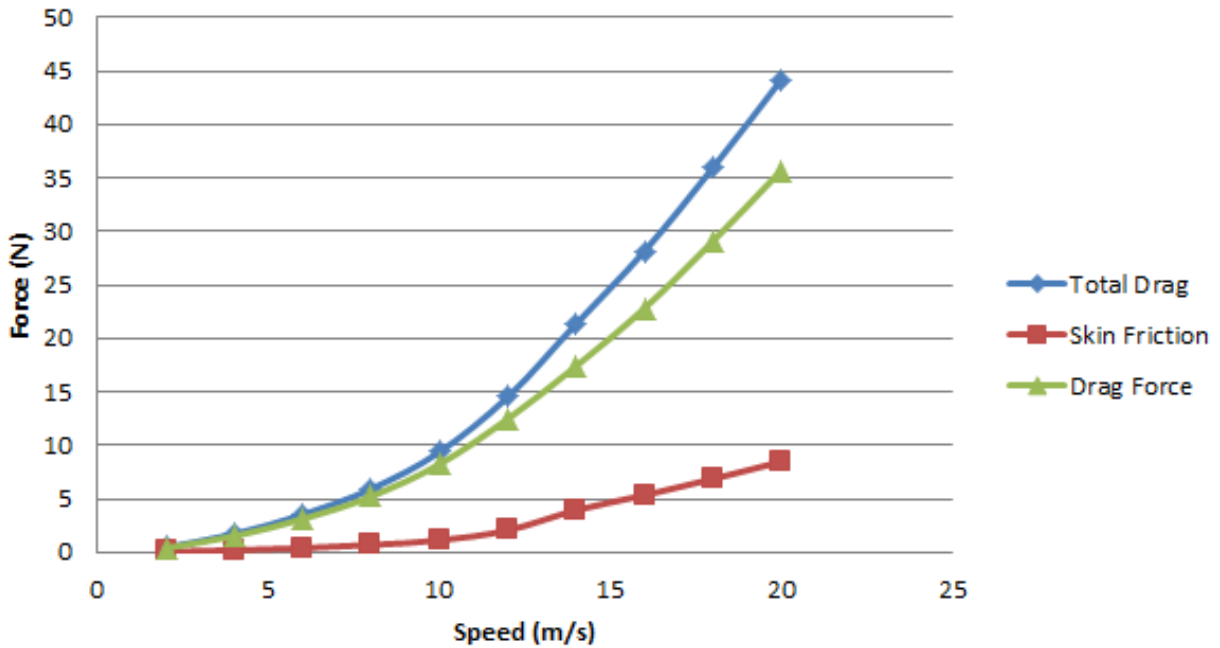


Figure C.4: Drag Force Curves Computed From SolidWorks Flow Simulation

The values of simulated drag were then sent into MATLAB and a curve fitting analysis was completed.

A graph of the raw data versus the fitted curve is shown in Figure C.4.

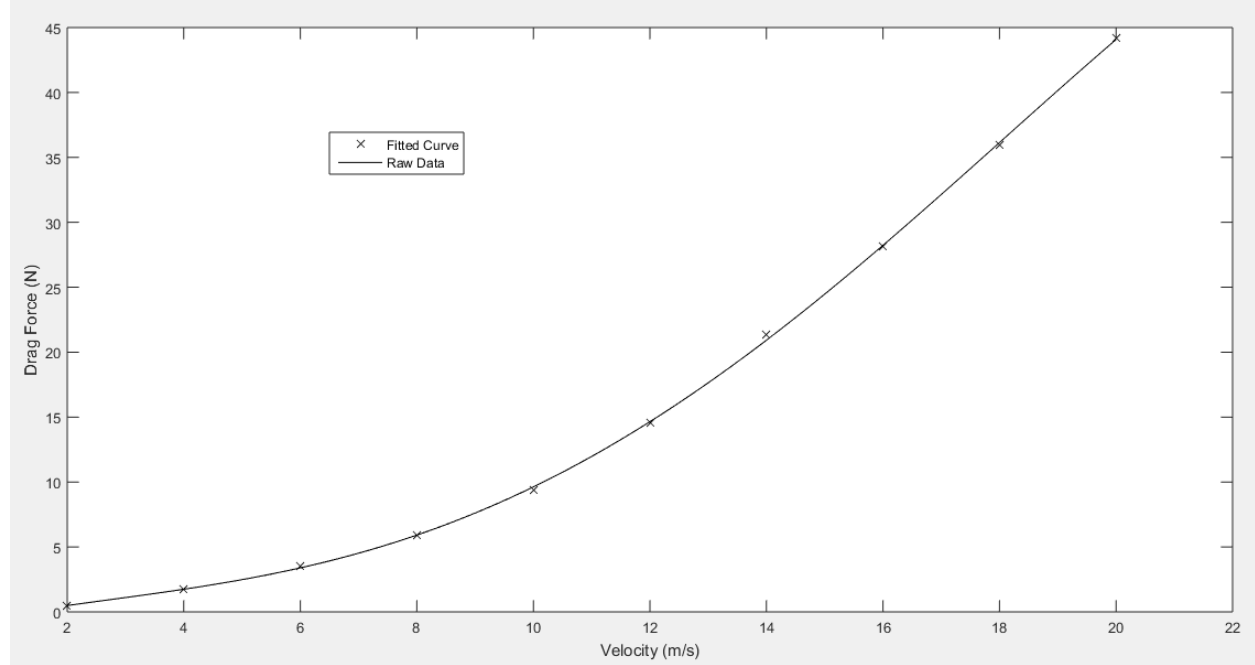


Figure C.5: Drag Force Curves Computed From SolidWorks Flow Simulation

The equation from the curve (generated from MATLAB) was found to be:

$$D(v) = -0.0003545v^4 + 0.014182v^3 - 0.05385v^2 + 0.45054v - 0.087259 \quad (\text{C.15})$$

Where D is the drag force and v is the airship speed, in m/s . Equation C.15 is what is used throughout the report to obtain drag forces.

Raw MATLAB code:

```

1 v=[0,2,4,6,8,10,12,14,16,18,20];
2 x=transpose(v);
3 d=[0,0.4663,1.7320,3.5236,5.9242,9.3913,14.5235,21.3659,28.1595,35.9296,44.1682];
4 y=transpose(d);
5 f=fit(x,y,'poly4');
6
7 cvalues = coeffvalues(f);
8 cnames = coeffnames(f);
9 output = formula(f);
10
11 for ii=1:1:numel(cvalues)
12     cname = cnames{ii};
13     cvalue = num2str(cvalues(ii));
14     output = strrep(output, cname, cvalue);

```

```

15 end
16
17 disp(output)
18
19 plot(f,'k',v,d,'xk'), xlabel('Velocity (m/s)'), ylabel('Drag Force (N)'), ...
20 legend('Fitted Curve', 'Raw Data')

```

C.11 New Drag Analysis

Once it was understood that the airship itself needed to be parametrizable, a new method of computed drag needed to be determined, as the simulations only accounted for the old airship dimensions. For this, an analysis from a report called *Technical Manual of Airship Aerodynamics* [30] was used. The following formula was used to compute drag:

$$D = C_D \rho (vol)^{2/3} v^{1.86} \quad (\text{C.16})$$

Where D is the drag in lbf (converted to N), ρ is the density of air [$slugs/ft^3$], vol is the volume of the airship envelope [ft^3], v is the velocity of the airship [ft/s], and C_D is the Prandtl Shape Coefficient. For this airship, C_D is estimated using Table C.3 below.

Table C.3: Airship Model Characteristics and Data [30]

Name of model	Length, L	Diameter, D	Surface, S	Area maximum cross-sectional area A	Volume, Vol.	Prandtl shape coefficient, C_D			Fineness ratio $F_R = \frac{L}{D}$	Distance maximum diameter from nose	Distance CG from nose	Prismatic coefficient, $Q = \frac{Vol.}{A \times L}$	Index of form efficiency, $H_F = \frac{Q}{C_D}$		
						20 m. p. h.	40 m. p. h.	60 m. p. h.					20 m. p. h.	40 m. p. h.	60 m. p. h.
Navy B (Goodrich)	3. 527	0. 6967	5. 800	0. 381	0. 8304	0. 0168	0. 0154	0. 0148	5. 060	37. 80	0. 6176	36. 76	40. 10	41. 73
Navy C	2. 919	. 6417	4. 750	. 323	. 6259	. 0159	. 0144	. 0136	4. 620	30. 00	46. 37	. 6562	41. 27	45. 57	48. 25
Navy E	4. 125	. 6417	5. 007	. 323	. 6690	. 0168	. 0146	. 0142	4. 870	36. 25	48. 64	. 6621
E. P.	3. 092	. 6417	4. 597	. 323	. 5890	. 0166	. 0147	. 0138	4. 820	41. 59	43. 92	. 6891	35. 49	40. 08	42. 70
I. E.	2. 985	. 6417	4. 597	. 323	. 5955	. 0175	. 0155	. 0144	4. 650	38. 18	44. 25	. 6169	35. 25	39. 80	42. 84
Goodyear-4 2	3. 190	. 6870	5. 470	. 371	. 7840	. 0162	. 0144	. 0134	4. 640	28. 76 6624	40. 89	45. 37	49. 43
Goodyear-1	3. 420	. 6660	5. 600	. 348	. 7360 0141	5. 130	34. 15	6184
Goodyear-2	3. 830	. 6350	6. 000	. 317	. 7520 0141	6. 020	36. 14	6194
Goodyear-3	3. 670	. 6150	5. 900	. 297	. 7760 0140	5. 970	36. 36	7119
Goodyear-4	3. 190	. 6870	5. 470	. 371	. 7840 0153	4. 640	28. 76	6624
Astra-Torres	3. 167	. 6914	5. 190	. 309	. 6583	. 0190	. 0159	. 0147	4. 583	33. 80	49. 08	. 6590	34. 68	41. 45	44. 83
Parseval P. I	3. 942	. 6417	5. 465	. 323	. 7240	. 0185	. 0174	. 0165	6. 140	38. 75	43. 19	. 5679	30. 70	32. 64	34. 42
Parseval P. II	3. 208	. 6417	4. 528	. 323	. 5891	. 0181	. 0170	. 0164	4. 990	38. 90	44. 46	. 5677	31. 36	33. 39	34. 62
Parseval P. III	3. 208	. 6417	4. 750	. 323	. 6331	. 0179	. 0169	. 0161	4. 699	47. 33	45. 85	. 6095	34. 05	36. 06	37. 86
Parseval S. S. T	5. 625	1. 1330	14. 720	1. 008	3. 4550	. 0174	. 0173	. 0170	4. 960	45. 00	45. 88	. 6090	35. 00	35. 23	35. 82
Pony Blimp AA	1. 992	. 5833	2. 760	. 267	. 3196	. 0205	. 0254	. 0277	3. 410	42. 50	46. 00	. 6003	29. 28	23. 63	21. 67
UB-FC	4. 9383	1. 0591	12. 9584	. 8810	2. 8693	. 0321	. 0223	. 0219	4. 663 65746
UB-2	4. 4894	1. 1638	12. 2240	1. 0633	2. 9201	. 0205	. 0189	. 0192	3. 823 61145
<i>C class cylindric midships</i>															
1/4 diameter	3. 109	. 6417	5. 073	. 323	. 6777	. 0154	. 0140	. 0132	4. 855 6749	43. 82	48. 21	51. 13
1/2 diameter	3. 270	. 6417	5. 398	. 323	. 7297	. 0153	. 0141	. 0135	5. 100 6909	45. 16	49. 00	51. 18
1 diameter	3. 590	. 6417	6. 043	. 323	. 8330	. 0164	. 0146	. 0136	5. 570 7184	43. 80	49. 21	52. 82
2 diameter	4. 232	. 6417	7. 337	. 323	1. 0404	. 0175	. 0150	. 0136	6. 600 7611	43. 49	50. 74	55. 96
3 diameter	4. 872	. 6417	8. 627	. 323	1. 2471	. 0173	. 0156	. 0148	7. 590 7925	45. 81	50. 80	53. 55
4 diameter	5. 515	. 6417	9. 922	. 323	1. 4548	. 0175	. 0157	. 0146	8. 590 8167	46. 67	52. 02	55. 94
5 diameter	6. 158	. 6417	11. 218	. 323	1. 6625	. 0164	. 0154	. 0148	9. 602 8358	50. 96	54. 27	56. 47

Various airship dimensions can be seen below here. The aircraft dimensions shown below were for

testing done in a wind tunnel to determine drag effects on real airships, so they are scaled down models. The goal is to select a model that has comparable dimensions to the airship we are using. As a starting point, the fineness ratio f is computed for our airship. As an estimate, $f = L/D \approx 3.6/1.2 = 3$. In reference to Table C.3, the closest match would be the Pony Blimp AA, with a fineness ratio of 3.4.

It can be deduced from the table that the Prandtl Shape coefficient encompasses both skin and form drag. When the fineness ratio is higher, skin friction drag will have a larger effect than form drag, so when the airspeed is increased (from 20mph to 60mph), C_D will decrease. The opposite is true with small fineness ratios, where the form drag plays a larger role, therefore the C_D increases as airspeed is increased. To be conservative, the highest C_D from the Pony Blimp AA, therefore $C_D = 0.0227$. An example calculation is shown below, for a windspeed of $20m/s$:

$$D = C_D \rho (vol)^{2/3} v^{1.86} = 0.0227 * (0.00237 \text{ slugs}/\text{ft}^3) * (122.644 \text{ ft}^3)^{2/3} (65.616 \text{ ft}/\text{s})^{1.86} = 3.183 \text{ lbf} = 14.1586 \text{ N}$$
(C.17)

The formula will be converted into metric units for simplicity, using a multiplication factor.

$$D = 0.847103 * (C_D) * (\rho[\text{kg}/\text{m}^3]) * (vol[\text{m}^3])^{2/3} * (v[\text{m}/\text{s}])^{1.86}$$
(C.18)

Based on Table C.4, the envelope contributes 45% to the drag. Therefore the total drag will be estimated as $D_{total} = D/0.45$. Based on this, the total drag is found in Equation C.17 is now 31.463 N

Table C.4: Drag Contribution for Various Airship Components [30]

(1) Large nonrigids with closed cars:		<i>Percent</i>
(a)	Envelope	45
(b)	Surfaces	20
(c)	Rigging and suspension cables	15
(d)	Cars	15
(e)	Accessories	5
(2) Small nonrigids with open cars:		
(a)	Envelope	35
(b)	Surfaces	25
(c)	Rigging and cables	20
(d)	Cars	15
(e)	Accessories	5

The value of C_D will change based on the fineness ratio. In the GUI of the MATLAB program, the user will select a fineness ratio from a drop-down menu, of 3.5, 4, and 4.5, followed by a total length of the blimp. To calculate the drag for these situations, the volume of the blimp will be computed, and the C_D will change based on the fineness ratio, as follows:

Table C.5: Fineness Ratios and Corresponding C_D

Fineness Ratio	C_D
3.5	0.0254
4	0.0189
4.5	0.0159

C.12 Gondola Hinge

sectionGondola Hinge The loading on the gondola hinge by forces $R_{x'}$ and $R_{z''}$ calculated in system modelling section ?? will be relatively small. Stress concentration would occur at points A and B shown in Figure C.6, however to avoid these stress concentrations fillets will be added to the part.

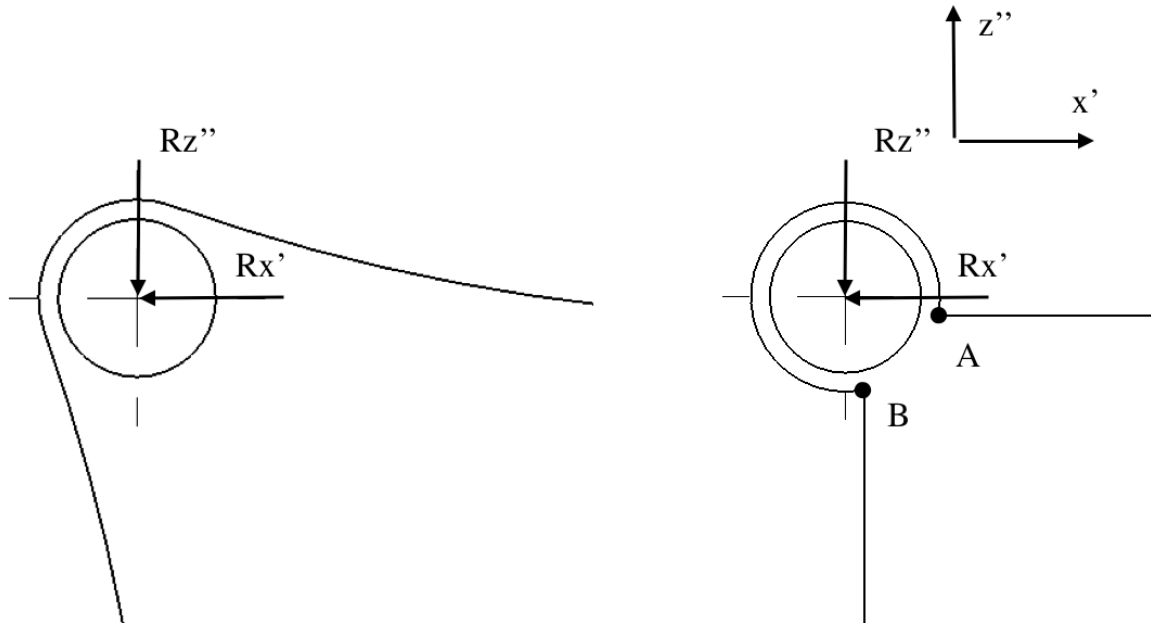


Figure C.6: Gondola Hinge Comparison Fillet Vs. No Fillet

The hinge pin will likely be made of aluminium and the shear stress experienced by the part will not be considerable relative to the strength of the material.

C.13 Thrust Force

Vectoring thrusters will be mounted to the both sides of the airship via the thruster supports attached to the keel. In order to encompass the forces that will be generated by the thruster, an equation will be used which was developed via research and experimental data collected and compiled by Gabriel Staples [29]. The basis of the equation is Newtons second law.

$$T = \frac{\partial(mv)}{\partial t} = \dot{m}v$$

based on this equation, in theory static thrust can be defined as

$$T_{static} = \dot{m}V_e$$

where V_e is the escape velocity of air through the thruster in m/s and \dot{m} is the mass flow of air through the thruster in kg/s . For dynamic thrust, which incorporates the movement of the airship,

$$T = \dot{m}\Delta V = \dot{m}(V_e - V_{as})$$

where V_{as} is the velocity of air coming into the thrusters in m/s but in a windless circumstance it is the airship velocity. Knowing that $\dot{m} = \rho A V_e$ and $A = \pi \frac{D^2}{4}$ where A is the area the propellers will cover in m^2 and D is the diameter of the propellers in m .

$$T = \rho \frac{\pi D^2}{4} (V_e^2 - V_e V_{as}) \quad (\text{C.19})$$

There is obviously some proportionality between the escape velocity V_e and the tip velocity of the propeller. This claim can be supported by the fact that the tangential velocity of a propeller blade will be increasing along its radius, therefore the greater the diameter the higher the tip speed. This velocity will affect the incident velocity of air it comes into contact with. Therefore a greater diameter will result in greater thrust as well as higher efficiency compared to a propeller of the same pitch with a lesser diameter [29]. This effect however tops out when the tip speed approaches the speed of sound.

Pitch will also affect both the thrust and efficiency. Lower pitch diameter results in lower angle of attack. Lower angle of attack means less separation, less induced drag, as a result, higher diameter and lower pitch props will typically be more efficient [29].

In order to incorporate this into equation C.19, V_e is replaced with V_{pitch} which equals $RPM \cdot Pitch \cdot \frac{1min}{60s}$ where RPM is the rotations per minute of the motor, and Pitch is the pitch di-

ameter of the propeller blade in m . Equation C.19 is multiplied by a constant coefficient and the propeller diameter to pitch ratio to the power of a constant, as seen below in equation C.20.

$$T = \rho \frac{\pi D^2}{4} \left(K_1 \left(\frac{D}{Pitch} \right)^{K_2} \right) \left(\left(RPM \cdot Pitch \cdot \frac{1min}{60s} \right)^2 - V_{as} \left(RPM \cdot Pitch \cdot \frac{1min}{60s} \right) \right) \quad (\text{C.20})$$

The assumption that $V_e \approx V_{pitch}$ is not accurate. In addition, it is assumed that the air velocity across the area of the thruster will be constant, when in reality this is not the case [29]. Some of the error derived from these assumptions is corrected by the coefficient term in C.20. In order to choose these coefficients, a study done by Gabriel Staples [29] [28], compares data calculated with equation C.20 using varying constants, with experimental static thrust data from more than 150 tests which were done by multiple sources. These were used along with theoretical dynamic thrust data [4], and a smaller sample of experimental dynamic thrust data. The values for K_1 and K_2 that resulted in calculated thrust forces that best matched the experimental data were 0.16716 and 1.5. Since these values were determined using mainly static thrust data, they are more accurate when calculating static thrust. The highest forces will be generated during low speed or static thrusting so these will be the values used when modeling the parts supporting the thrusters. Results from comparing thrust values calculated using Gabriel Staples's equation C.21 and experimental data for both static and dynamic thrust can be found in appendix section C.13, Figures C.8 and C.9.

The following equation shows a sample calculation using an achievable motor RPM of 11000 from the HobbyKing 2612 Brushless Outrunner Motor 1900KV, whose specs can be seen in appendix section D.6.1. This RPM value was based off results obtained from an online calculator comparing required power values at varying RPMs to the power shown in appendix section C.13, Figures C.10. An airship speed of 10m/s was used.

$$T = \rho \frac{\pi D^2}{4} \left(0.16716 \left(\frac{D}{Pitch} \right)^{1.5} \right) \left(\left(RPM \cdot Pitch \cdot \frac{1min}{60s} \right)^2 - V_{as} \left(RPM \cdot Pitch \cdot \frac{1min}{60s} \right) \right) \quad (\text{C.21})$$

$$\begin{aligned} &= 1.225[\text{kg/m}^3] \frac{\pi(0.1778[m])^2}{4} \left(0.16716 \left(\frac{0.1778[m]}{0.127[m]} \right)^{1.5} \right) \left(\left(11000[\text{rpm}] \cdot 0.127[m] \cdot \frac{1min}{60s} \right)^2 \right. \\ &\quad \left. - 10[m/s] \left(11000[\text{rpm}] \cdot Pitch \cdot \frac{1min}{60s} \right) \right) = 2.604[N] \end{aligned}$$

Appendix section C.13, Figure C.7 depicts the decrease in thrust force with increasing airship speed. This phenomena can also be observed below in table C.6. At an RPM of 11000 as the air ship reaches 24m/s the thrust force goes to 0 indicating that this would be the maximum speed. Obviously there are several considerable forces such as gravitational forces, drag, and other aerodynamic forces which are not

accounted and this is therefore not an accurate method of determining maximum speed.

Table C.6: Table of Calculated Thrust Values for Varying Airship Speeds

Airship Speed, V_{as} , (m/s)	Airship Speed, V_{as} (mph)	Thrust, T (N)	Thrust, T (g)	Thrust, T (kg)
0	0.000	4.566	465.403	0.465
1	2.237	4.370	445.414	0.445
2	4.474	4.173	425.425	0.425
3	6.711	3.977	405.436	0.405
4	8.948	3.781	385.448	0.385
5	11.185	3.585	365.459	0.365
6	13.422	3.389	345.470	0.345
7	15.659	3.193	325.482	0.325
8	17.896	2.997	305.493	0.305
9	20.132	2.801	285.504	0.286
10	22.369	2.605	265.516	0.266
11	24.606	2.409	245.527	0.246
12	26.843	2.213	225.538	0.226
13	29.080	2.016	205.550	0.206
14	31.317	1.820	185.561	0.186
15	33.554	1.624	165.572	0.166
16	35.791	1.428	145.584	0.146
17	38.028	1.232	125.595	0.126
18	40.265	1.036	105.606	0.106
19	42.502	0.840	85.617	0.086
20	44.739	0.644	65.629	0.066
21	46.976	0.448	45.640	0.046
22	49.213	0.252	25.651	0.026
23	51.450	0.056	5.663	0.006
24	53.687	-0.141	-14.326	-0.014

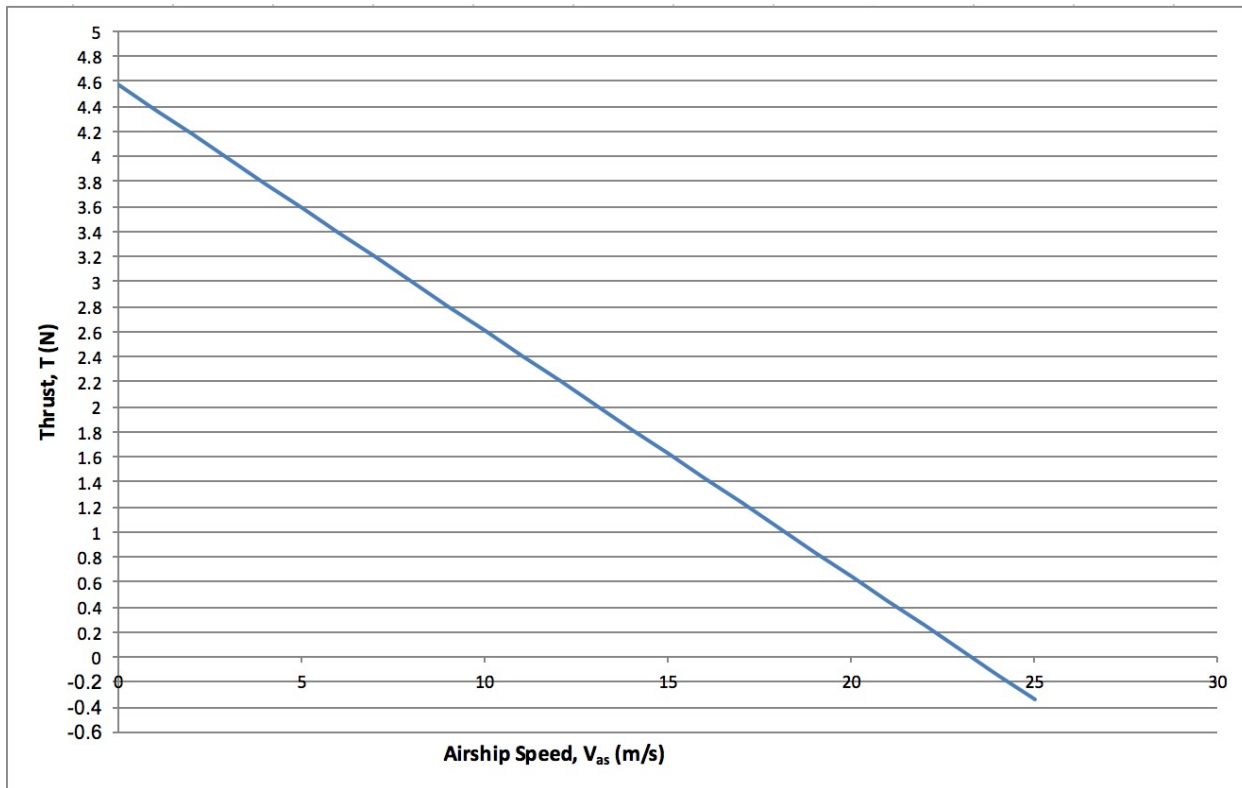


Figure C.7: Graph of Thrust Plotted Against Airship Speed at 11000rpm With 7", 5" Pitch Diameter Propeller

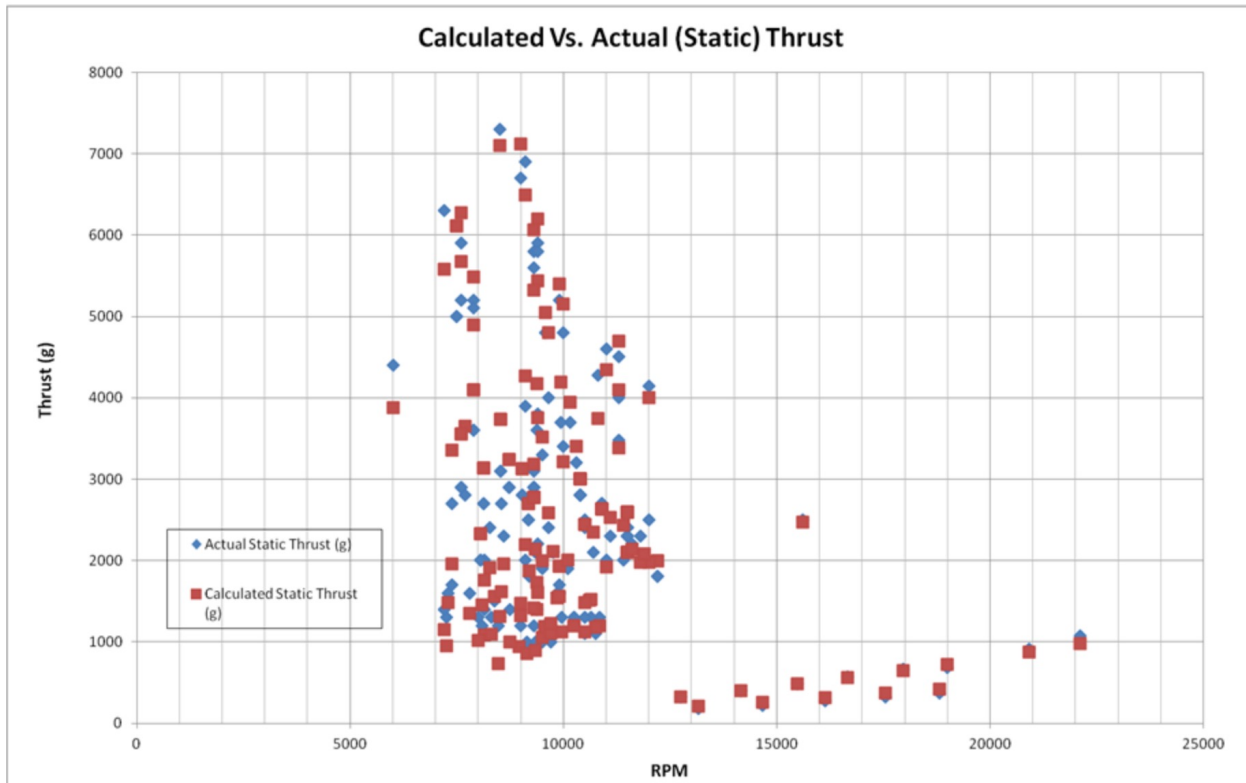


Figure C.8: Test Data from Gabriel Staples Against Experimental Static Thrust Values [29]

Propeller Dynamic Thrust - Experimental Results vs. Semi-empirical Calculation

10x6 propeller, Full Throttle

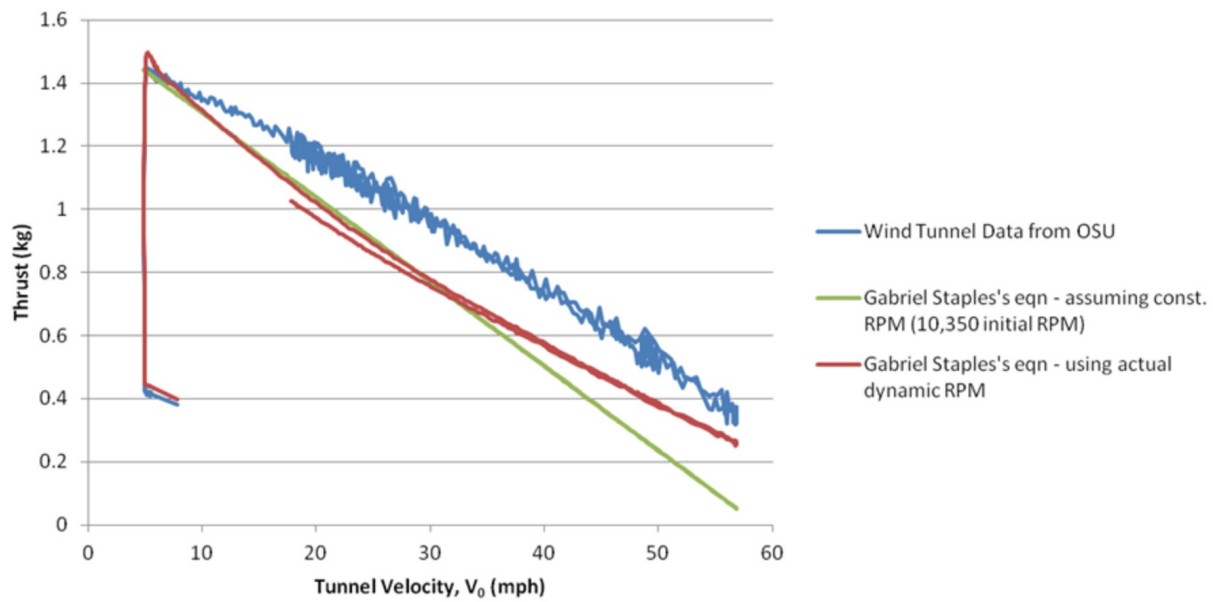


Figure C.9: Test Data from Gabriel Staples Against Experimental Dynamic Thrust Values [29]

Propeller diameter	7	inch
Pitch	5	inch
Propeller type	Standard propeller <input type="button" value="▼"/>	
	CF <input type="button" value="1"/>	
No. of blades	2	<input type="button" value="▼"/>
RPM	11000	
Air temperature	68 Fahrenheit <input type="button" value="▼"/>	
Air density	1.2045 (kg/m ³)	
Static thrust = 12.34 oz		
Static thrust = 0.79 pound		
Static thrust = 0.35 kg		
Perimeter speed = 102.35 m/s		
Required engine power = 0.108 HP = 0.079 kW		
Estimated flying speed = 52.0 mph = 45.1 Knots		

Figure C.10: Sample Thrust Calculation Using On-line Calculator [7]

Appendix D: Data Sheets

D.1 Linear Actuator [1]



100mm L12 Actuator
Actual Size

Benefits

- Compact
- Simple control
- Low voltage
- Equal push/pull
- Easy mounting

Applications

- Robotics
- Appliances
- Toys
- RC vehicles
- Automotive
- Industrial Automation

Miniature Linear Motion Series · L12

Actuonix Motion Devices unique line of Miniature Linear Actuators enables a new generation of motion-enabled product designs, with capabilities that have never before been combined in a device of this size. These small linear actuators are a superior alternative to designing with awkward gears, motors, servos, and linkages.

Actuonix's L series of micro linear actuators combine the best features of our existing micro actuator families into a highly flexible, configurable, and compact platform with an optional sophisticated on-board microcontroller. The first member of the L series, the L12, is an axial design with a powerful drive-train and a rectangular cross section for increased rigidity. But by far the most attractive feature of this actuator is the broad spectrum of available configurations.

L12 Specifications

Gearing Option	50:1	100:1	210:1
Peak Power Point	17N @ 14mm/s	31N @ 7mm/s	62N @ 3.2mm/s
Peak Efficiency Point	10N @ 19mm/s	17N @ 10mm/s	36N @ 4.5mm/s
Max Speed (<i>no load</i>)	25mm/s	13mm/s	6.5mm/s
Max Force (<i>lifted</i>)	22N	42N	80N
Back Drive Force (<i>static</i>)	12N	22N	45N
Stroke Option	10 mm	30mm	50mm
Mass	28 g	34 g	40 g
Repeatability (-I, -R, -P&LAC)	±0.1 mm	±0.2 mm	±0.3 mm
Max Side Load (<i>extended</i>)	50N	40N	30N
Closed Length (<i>hole to hole</i>)	62mm	82mm	102mm
Potentiometer (-I, -R, -P)	1kΩ±50%	3kΩ±50%	6kΩ±50%
Voltage Option	6VDC	12VDC	
Max Input Voltage	7.5V	13.5V	
Stall Current	460mA	185mA	
Standby Current (-I/-R)	7.2mA	3.3mA	
Operating Temperature	-10°C to +50°C		
Potentiometer Linearity	Less than 2.00%		
Max Duty Cycle	20 %		
Audible Noise	55dB @ 45cm		
Ingress Protection	IP-54		
Mechanical Backlash	0.2mm		
Limit Switches (-S)	Max. Current Leakage: 8uA		
Maximum Static Force	200N		

1 - Control Option Specific values are identified with -I, -R, -P, -S, and LAC

2 - 1 N (Newton) = 0.225 lbf (pound-force) & 25.4mm=1 Inch

3 - A powered-off actuator will statically hold a force up to the Backdrive Force

4 - Actuators should be tested in each specific application to determine their effective life under those loading conditions and environment.

All information provided on this datasheet is subject to change. Purchase or use of Actuonix actuators is subject to acceptance of our terms and conditions as posted here: <http://www.actuonix.com/terms.asp>



Actuonix Motion Devices Inc

580 Starling Lane

Victoria, BC, V9E 2A9

Canada

1(206) 347-9684 phone

1(888) 225-9198 toll-free

1(206) 347-9684 fax

sales@actuonix.com

Copyright 2016 © Actuonix Motion Devices Inc.

D.2 Bearings [20]

10/10/2017

McMaster-Carr - General Purpose Plastic Ball Bearing, with Stainless Steel Ball, for 1/4" Shaft Diameter, 5/8" OD



General Purpose Plastic Ball Bearing with Stainless Steel Ball, for 1/4" Shaft Diameter, 5/8" OD

In stock
\$6.03 Each
6455K2



Bearing Type	Ball
For Load Direction	Radial
Ball Bearing Type	Standard
Construction	Single Row
Seal Type	Open
For Shaft Shape	Round
Trade No.	R4
For Shaft Diameter	1/4"
ID	0.25"
ID Tolerance	0" to 0.003"
OD	5/8"
OD Tolerance	-0.003" to 0"
Width	0.196"
Width Tolerance	-0.005" to 0.005"
Material	Acetal
Cage Material	Plastic
Radial Load Capacity, lbs.	
Dynamic	25
Static	15
Maximum Speed	2,300 rpm
Shaft Mount Type	Press Fit
Lubrication	Not Required
Temperature Range	-40° to 180° F
ABEC Rating	Not Rated
Radial Clearance	0.001" to 0.008"
Ball Material	Stainless Steel
RoHS	Compliant

Choose these acetal bearings for their all-around corrosion and chemical resistance.

Stainless steel balls offer excellent corrosion resistance.

D.3 Friction Wheel Assembly

D.3.1 Friction Wheel [19]

10/10/2017

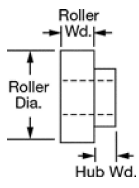
McMaster-Carr - Neoprene Roller, Drive, Aluminum Hub, 5/8" Roller Diameter, 3/16" Roller Width



Neoprene Roller

Drive, Aluminum Hub, 5/8" Roller Diameter, 3/16" Roller Width

In stock
\$16.70 Each
60885K31



Guide Roller Type	Drive
Roller Style	Shaft Mount
Roller Profile	Flat
Roller Material	Neoprene
Hub Material	Aluminum
Roller	
Diameter	5/8"
Width	3/16"
For Shaft Diameter	1/4"
Hub	
Diameter	1/2"
Width	1/4"
Shaft Mount Type	Set Screw
Set Screws	
Number Required	1
Included	No
Thread Size	8-32
Temperature Range	-40° to 170° F
Durometer (Hardness Rating)	55A (Medium) Black
RoHS	Compliant
Related Product	8-32 Stainless Steel Cup Point Set Screws (100/Pkg.)

Made of neoprene rubber, these rollers resist oil, flames, gasoline, and weather. Also known as contact wheels and feed rollers, they have tapped hubs that allow you to mount them onto a shaft or stud to transmit power.

D.3.2 Friction Wheel Set Screw [21]

10/10/2017

McMaster-Carr - Alloy Steel Cup-Point Set Screw, Black Oxide, 8-32 Thread, 1/4" Long



Alloy Steel Cup-Point Set Screw
Black Oxide, 8-32 Thread, 1/4" Long

In stock
\$10.65 per pack of 100
91375A190



Material	Black-Oxide Alloy Steel
Thread Size	8-32
Length	1/4"
Drive Size	5/64"
Screw Size Decimal Equivalent	0.164"
Hardness	Rockwell C45
Specifications Met	ASME B18.3, ASTM F912
Thread Type	UNC
Thread Spacing	Coarse
Thread Fit	Class 3A
Thread Direction	Right Hand
Drive Style	Hex
Tip Type	Cup
Head Type	Headless
System of Measurement	Inch
RoHS	Compliant

Made from alloy steel, these set screws have a thin edge that digs into hard surfaces for a secure hold. Length listed is the overall length.

Black-oxide alloy steel set screws resist corrosion in dry environments.

D.3.3 Friction Wheel Motor [24]

10/10/2017

Pololu - 50:1 Micro Metal Gearmotor HP 6V

50:1 Micro Metal Gearmotor HP 6V



www.pololu.com

Pololu item #: 998 438 in stock

Price break	Unit price (US\$)
1	15.95
10	13.55
50	11.96

Quantity: Add to cart[backorders allowed](#) Add to wish list

This gearmotor is a miniature **high-power, 6 V** brushed DC motor with a **51.45:1** metal gearbox. It has a cross section of 10 × 12 mm, and the D-shaped gearbox output shaft is 9 mm long and 3 mm in diameter.

Key specs at 6 V: 625 RPM and 120 mA with no load, 15 oz-in (1.1 kg-cm) and 1.6 A at stall.

Select options:

[Description](#) [Specs \(10\)](#) [Pictures \(20\)](#) [Resources \(12\)](#) [FAQs \(1\)](#) [On the blog \(1\)](#)

Dimensions

Size:	10 × 12 × 26 mm ¹
Weight:	9.5 g
Shaft diameter:	3 mm ²

General specifications

Gear ratio:	51.45:1
Free-run speed @ 6V:	630 rpm
Free-run current @ 6V:	120 mA
Stall current @ 6V:	1600 mA
Stall torque @ 6V:	15 oz·in
Extended motor shaft?:	N

<https://www.pololu.com/product/998/specs>

1/2

Table D.1: Various Gearing For Gondola Motor Torque [24].

6 V	high-power (HP) <i>(same specs as 6V HPCB above)</i>	1600 mA	6000 RPM	2 oz-in	<u>5:1 HP 6V</u>	<u>5:1 HP 6V dual-shaft</u>
			3000 RPM	4 oz-in	<u>10:1 HP 6V</u>	<u>10:1 HP 6V dual-shaft</u>
			1000 RPM	9 oz-in	<u>30:1 HP 6V</u>	<u>30:1 HP 6V dual-shaft</u>
			625 RPM	15 oz-in	<u>50:1 HP 6V</u>	<u>50:1 HP 6V dual-shaft</u>
			400 RPM	22 oz-in	<u>75:1 HP 6V</u>	<u>75:1 HP 6V dual-shaft</u>
			320 RPM	30 oz-in	<u>100:1 HP 6V</u>	<u>100:1 HP 6V dual-shaft</u>
			200 RPM	40 oz-in	<u>150:1 HP 6V</u>	<u>150:1 HP 6V dual-shaft</u>
			140 RPM	50 oz-in	<u>210:1 HP 6V</u>	<u>210:1 HP 6V dual-shaft</u>
			120 RPM	60 oz-in	<u>250:1 HP 6V</u>	<u>250:1 HP 6V dual-shaft</u>
			100 RPM	70 oz-in	<u>298:1 HP 6V</u>	<u>298:1 HP 6V dual-shaft</u>
			32 RPM	125 oz-in	<u>1000:1 HP 6V</u>	<u>1000:1 HP 6V dual-shaft</u>

D.3.4 Friction Wheel Encoder [25]

10/10/2017

Pololu - Magnetic Encoder Pair Kit for Micro Metal Gearmotors, 12 CPR, 2.7-18V (HPCB compatible)

Magnetic Encoder Pair Kit for Micro Metal Gearmotors, 12 CPR, 2.7-18V (HPCB compatible)

Pololu item #: 3081 **574** in stock

Price break	Unit price (US\$)
1	8.95
10	7.95
50	6.95

Quantity: **Add to cart**

backorders allowed **Add to wish list**

◀ ▶

Add quadrature encoders to your micro metal gearmotors (extended back shaft version required) with this kit that uses a magnetic disc and hall effect sensors to provide 12 counts per revolution of the motor shaft. The sensors operate from 2.7 V to 18 V and provide digital outputs that can be connected directly to a microcontroller or other digital circuit. This module is compatible with **all** of the dual-shaft micro metal gearmotors we carry, including the HPCB versions.

[Description](#) [Specs \(6\)](#) [Pictures \(13\)](#) [Resources \(5\)](#) [FAQs \(0\)](#) [On the blog \(4\)](#)

Overview

This kit includes two dual-channel Hall Effect sensor boards and two **6-pole magnetic discs** that can be used to add quadrature encoding to two **micro metal gearmotors with extended back shafts** (motors are not included with this kit). The encoder board senses the rotation of the magnetic disc and provides a resolution of 12 counts per revolution of the motor shaft when counting both edges of both channels. To compute the counts per revolution of the gearbox output shaft, multiply the gear ratio by 12.

D.3.5 Example Cable Gland [17]



DATA SHEET	53111000
SKINTOP® ST-M / STR-M	valid from : 21.07.2017

The polyamide based SKINTOP® ST-M / STR-M is designed for universal use, above all for functional safety in manufacturing of machines and equipment, in measurement and control technology and automation technology, as well as in the electronic technology and in manufacturing of robots.



Components:

Gland body	Polyamide, V-2 acc. to UL 94
Cap nut	Polyamide, V-2 acc. to UL 94
Sealing ring	CR (ozone- and UV-resistant)
O-Ring (M40x1,5 - M63x1,5)	NBR (ozone- and UV-resistant)

Technical features:

Connecting thread	M12x1,5 up to M63x1,5 acc. to EN 60423
Functional thread	Multi-start trapezoidal thread
Protection class IP / NEMA Enclosure types	IP68 – 5 bar/30 min, test acc. to EN 60529 IP69 acc. to EN 60529 NEMA Type 1 and Type 12
Strain relief:	Kat. A acc. to DIN EN 62444
Temperature range:	Dynamic -20 °C up to +100 °C Statically -40 °C up to +100 °C
Design	ST-M standard STR-M with reducing sealing ring (for smaller cable diameters)
Colour	RAL 7001 silver-grey RAL 7035 light-grey RAL 9005 black, UV-resistant

Other characteristics:

Permanent vibration protection
Optimal strain relief
Large variable clamping ranges
M40 - M63 with O-ring

Approvals:



File Nr. 79903

Norm references:

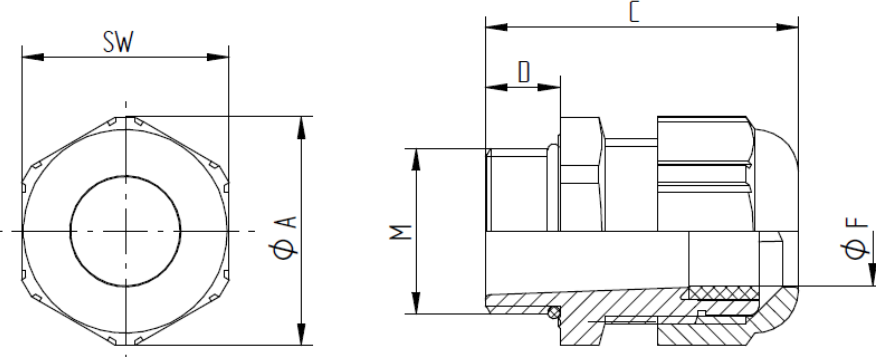


For more information please see our current catalogue.

elaborated by: PDP: T. Dvoulety	Document: DB53111000_11EN	page 1 of 2
------------------------------------	---------------------------	-------------



DATA SHEET		53111000
SKINTOP® ST-M / STR-M		valid from : 21.07.2017



SKINTOP® ST-M

M	SW [mm]	Ø A [mm]	C [mm]		D [mm]	Ø F [mm] Clamping range	O-Ring [mm]	Article No.		
			min.	max.				RAL 7001	RAL 7035	RAL 9005
M12x1,5	15	16,6	26,5	30	8	3,5 - 7	-	53111000	53111400	53111200
M16x1,5	19	21,1	29	34	8	4 - 10	-	53111010	53111410	53111210
M20x1,5	25	27,6	34	37	9	6 - 13	-	53111020	53111420	53111220
M25x1,5	30	33,6	35	40	10	8 - 17	-	53111030	53111430	53111230
M32x1,5	36	40,3	39	47	10	9 - 21	-	53111040	53111440	53111240
M40x1,5	46	51,6	43	52	10	16 - 28	36 x 2	53111050	53111450	53111250
M50x1,5	55	61,6	54	62	12	27 - 34	46 x 2	53111060	53111460	53111260
M63x1,5	66	73,9	59	71	12	34 - 45	57 x 2	53111070	53111470	53111270

SKINTOP® STR-M

M	SW [mm]	Ø A [mm]	C [mm]		D [mm]	Ø F [mm] Clamping range	O-Ring [mm]	Article No.		
			min.	max.				RAL 7001	RAL 7035	RAL 9005
M12x1,5	15	16,6	26,5	30	8	2 - 5	-	53111100	53111500	53111300
M16x1,5	19	21,1	29	34	8	3,5 - 7	-	53111110	53111510	53111310
M20x1,5	25	27,6	34	37	9	4 - 10	-	53111120	53111520	53111320
M25x1,5	30	33,6	35	40	10	5 - 13	-	53111130	53111530	53111330
M32x1,5	36	40,3	39	47	10	6 - 15	-	53111140	53111540	53111340
M40x1,5	46	51,6	43	52	10	9 - 23	36 x 2	53111150	53111550	53111350
M50x1,5	55	61,6	54	62	12	24 - 29	46 x 2	53111160	53111560	53111360
M63x1,5	66	73,9	59	71	12	28 - 39	57 x 2	53111170	53111570	53111370

elaborated by: PDP: T. Dvoulety	Document:	DB53111000_11EN	page 2 of 2
------------------------------------	-----------	-----------------	-------------

D.4 Spring [22]

10/10/2017

McMaster-Carr - Music-Wire Steel Torsion Spring, 180 Degree Right-Hand Wound, 0.767" OD



Music-Wire Steel Torsion Spring 180 Degree Right-Hand Wound, 0.767" OD

In stock
\$8.06 per pack of 6
9271K271



Spring Type	Torsion
Material	Music-Wire Steel
Deflection Angle	180°
Wind Direction	Right Hand
OD	0.767"
For Maximum Shaft Diameter	0.500"
Wire Diameter	0.063"
Leg Length	2,000"
Number of Coils	6.00
Spring Length @ Maximum Torque	0.475"
Maximum Torque	5,518 in.-lbs.
RoHS	Compliant

These music-wire steel springs are stronger than stainless steel springs. Commonly found in clothespins, spring clamps, mousetraps, motors, and spring-return mechanisms, torsion springs maintain pressure over a short distance in a rotational direction. They are often supported by a shaft, mandrel, or arbor.

Squeezing a torsion spring reduces its OD, which tightens the spring around a shaft and increases the spring length. Since the spring gets tighter as it is squeezed around the shaft, a maximum shaft diameter for each spring is listed. Using a shaft with a larger diameter will interfere with the spring motion.

Torsion springs should be used in the direction in which the coils are wound. Deflection angle represents the angle between the legs of the spring as well as the maximum spring rotation. All springs rotate until their legs are parallel. For example, a spring with a 90° deflection angle has a 90° angle between its legs, and it will rotate a maximum of 90°. Maximum torque is the torque required to rotate the spring legs to the parallel position.

D.5 Battery [8]

Rhino 2250mAh 3S 11.1v 40C Lipoly Pack



Specifications

SKU:	R2250-40-3	Brand:	N/A
Weight(g)	243.00	Length	109.00
Width:	26.00	Height:	36.00
Capacity (mAh)	2250.00	Discharge(c)	40.00
Length-A(mm):	107.00	Height-B(mm):	34.00
Width-C(mm)	26.00	Unit Weight (g)	191
Max Charge Rate(C):	5.00	Discharge Plug:	N/A

D.6 Thruster Assembly

D.6.1 Thruster Motor [15]

HobbyKing®™ 2612 Brushless Outrunner 1900KV



Specifications

RPM/V: **1900Kv**
Cell Count: **2~3s Lipoly**
Max.efficiency: **78.0%**
Current at Max.eff: **6.3~8.7A**
Max.current: **14A**
No Load Current: **0.8A/7V**
Internal Resistance: **165mOhm**
Diameter: **27mm**
Length: **23.4mm**
Mounting Hole Spacings: **32mm**
Mounting Hole Diameter: **2mm**
Shaft: **3mm**
Weight: **25g**

D.6.2 Propeller [13]

Aerostar Carbon Fibre Propeller 7x5



Specifications

SKU:	9445000180-0	Brand:	N/A
Weight(g)	14.00	Length	180.00
Width:	15.00	Height:	20.00
Pitch Y(inch)	5.00	Material	Carbon Fiber
Rotation:	CCW	Unit Weight (g):	N/A
Type	Normal	Blade Count	2
Diameter X(inch):	7.00		

D.6.3 BEC [9]

TURNIGY Plush 10amp Speed Controller w/BEC



Specifications

Cont Current: 10A	SKU:	TR_P10A
Burst Current: 12A	Weight(g)	20.00
BEC Mode: Linear	Width:	10.00
BEC : 5v / 2A	Brand:	No
Lipo Cells: 2-4	Length	110.00
NiMH : 5-12	Height:	110.00
Weight: 9g		
Size: 27x17x6mm		

D.6.4 Servo Motor [26]

RB-Hit-128

HS-7950TH Ultra Torque HV Coreless Titanium Gear Servo



Hitec's strongest servo period, the "Ultra Torque" HS-7950TH is designed to operate on a two cell LiPo Pack. Featuring our high resolution "G2" second generation programmable digital circuit and our indestructible Titanium gears, the HS-7950TH has the performance and durability you've come to expect from a Hitec servo. Other features in the HS-7950TH include a 7.4V optimized coreless motor, integrated heat sink case, and a top case with two hardened steel gear pins supported by axial brass bushing.

The HS-7950TH has been designed for the most demanding hobby applications including the largest aircraft and monster trucks. Featuring a titanic 403 oz./in. of torque at 6.0 volts, while still maintaining a respectable 0.15 second transit time.

Features

- G2 Digital Circuit
- Titanium Gear Train (MK first gear)

- Ultra Performance Coreless Motor
- Heatsink Case
- (8) O-Rings for Water/Dust/Fuel protection
- Dual Ball Bearing Supported Output Shaft

Programmable Features Include:

- Dead Band Width
- Direction of Rotation
- Speed of Rotation (slower)
- End Points
- Neutral Points
- Fail Safe On/Off
- Fail Safe Point
- Resolution* (default is high resolution)
- Overload Protection* (default is off)

Specifications

- Motor Type: Coreless
- Bearing Type: Dual Ball Bearing
- Speed (6.0V/7.4V): 0.15 / 0.13
- Torque oz./in. (6.0V/7.4V): 403 / 486
- Torque kg./cm. (6.0V/7.4V): 29.0 / 35.0
- Size in Inches: 1.57 x 0.79 x 1.50
- Size in Millimeters: 39.88 x 20.07 x 38.10
- Weight oz.: 2.40
- Weight g.: 68.04

D.6.5 Receiver [14]

FrSky TFR6M 2.4Ghz 6CH Micro Receiver FASST Compatible



Specification

SKU:	236000003	Brand:	FrSky
Weight(g)	34.00	Length	160.00
Width:	20.00	Height:	87.00

D.7 Flight Control Assembly

D.7.1 ESC [10]

Turnigy 20A BRUSHED ESC



Specifications

SKU:	TGY-20A	Brand:	No
Weight(g)	39.00	Length	150.00
Width:	10.00	Height:	110.00

D.7.2 GPS Module [12]

UBLOX Micro M8N GPS Compass Module

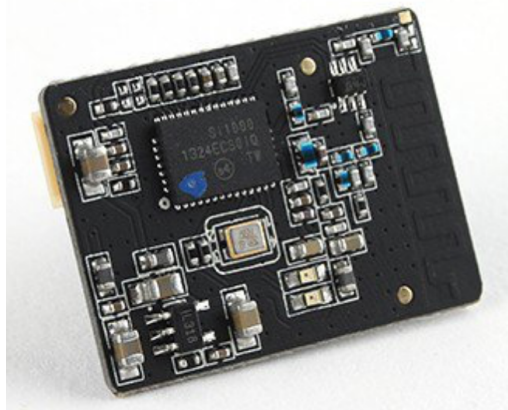


Specifications

SKU:	9387000083-0	Brand:	No
Weight(g)	29.00	Length	80.00
Width:	10.00	Height:	60.00

D.7.3 Transceiver [16]

Micro HKPilot Telemetry Radio Set with Integrated PCB
Antenna 915Mhz



Specifications

Supply voltage: **3.7-6 VDC**

Transmit current: **100 mA at 20 dBm**

Receive current: **25 mA**

Serial interface: **3.3 V UART**

Size: **19x25x5mm (with antenna)**

Weight: **1.6g (with antenna)**

Specs Ground Transceiver:

Supply voltage: **3.7-6 VDC (from USB or DF13 connector)**

Transmit current: **100 mA at 20 dBm**

Receive current: **25 mA**

Serial interface: **3.3 V UART**

Size: **25.5x 53x11 mm (without antenna)**

Weight: **11.5g (without antenna)**

SKU:	387000067-0	Brand:	No
Weight(g)	44.00	Length	100.00
Width:	40.00	Height:	70.00

D.7.4 Flight Controller [11]

PixFalcon Micro PX4 Autopilot



Specifications

SKU:	9387000082-0	Brand:	N/A
Weight(g)	99.00	Length	107.00
Width:	40.00	Height:	74.00

Appendix E: Engineering Drawings

E.1 Parts List

E.2 Complete System Drawing

including cross sections

E.3 Sub-Assembly Drawings

E.4 Individual Part Drawings

Appendix F: Meeting Minutes

F.1 Group Meeting Minutes

Group Minutes					
Attendees:		Absent:	Date & Time:	Venue:	
Alex Pennell (apenn095@uottawa.ca,7334789) Isaak Goldenberg (igold093@uottawa.ca,7395188) Joey Kane (jkane035@uottawa.ca,7386330) Sawyer Woodside (swood079@uottawa.ca,7158568)		none	10:30 am 6-Sept-2017	CBYB02	
Minute taker: Who is filling out this form?		Sawyer Woodside	Chairperson: Who is organising the meeting?	Sawyer Woodside	
	Task What has to be done?	Action What action is required to get it done?	Who Who is responsible?	Duration How long will it take to complete?	Status Has the task been completed?
1	Formatting Report	Pick software, organize template	Joey, Isaak	2 hours	No
2	Find Images	Write descriptions of the different parts, function, history, etc.	All	Ongoing	No
3	Filing	Set up a Google drive	Alex	1 hour	Yes
4	Meeting and Minutes	Decided chair person and taker are the same. Weekly rotation, setup schedule.	Sawyer	1 hour	Yes
5	Messaging	Setup Slack software	Sawyer	10 minutes	Yes
Next meeting Chairperson: Sawyer Woodside		Minute taker: Sawyer Woodside	Date & Time: 11:30am 8-Sept-2017	Venue: CBY B02	

Group Minutes					
Attendees: Alex Pennell (apenn095@uottawa.ca,7334789) Isaak Goldenberg (igold093@uottawa.ca,7395188) Joey Kane (jkane035@uottawa.ca,7386330)		Absent: Sawyer Woodside	Date & Time: 08:30 am 13-Sept-2017	Venue: CBYB02	
Minute taker: Who is filling out this form? Alex Pennell		Chairperson: Who is organising the meeting? Alex Pennell			
	Task What has to be done?	Action What action is required to get it done?	Who Who is responsible?	Duration How long will it take to complete?	Status Has the task been completed?
1	Read through other blimp designs	Use the references in the journal to find other designs	Joey	4 Hours	In progress
2	Write section on basic design	Find relevant pictures to use as reference and put in document	Isaak	6 Hours	In progress
3	Research attaching the gondola to keel and how it can move	Find relevant picture	Alex	6 Hours	In progress
4	Research and summarize regulations	Read through FAA guidelines for airships	Sawyer	6 Hours	In progress
5	Write scope and mandate	Start and finish the scope and mandate	Isaak	2 Hours	Complete
Next meeting Chairperson: Alex Pennell	Minute taker: Alex Pennell		Date & Time: 11:30am 13-Sept-2017	Venue: CBY B02	

Group Minutes					
Attendees: Alex Pennell (apenn095@uottawa.ca,7334789) Isaak Goldenberg (igold093@uottawa.ca,7395188) Joey Kane (jkane035@uottawa.ca,7386330) Sawyer Woodside (swood079@uottawa.ca,7158568)		Absent: none	Date & Time: 11:30 am 19-Sept-2017	Venue: DMS	
Minute taker: Isaak Goldenberg Who is filling out this form?		Chairperson: Who is organising the meeting?	Alex Pennell		
Task What has to be done?	Action What action is required to get it done?	Who Who is responsible?	Duration How long will it take to complete?	Status Has the task been completed?	
1 Get rough gondola design ideas	Brainstorm based off of literature review	Alex, Sawyer	6 Hours	No	
2 Get quote for keel	Put rough 3D out for quotes	Sawyer	1 Hour	Yes	
3 Get rough dimensions and weights of equipment needed	Find the required components data sheets	Joey, Isaak	6 Hours	No	
4					
5					
Next meeting Chairperson: Isaak Goldenberg	Minute taker: Isaak Goldenberg	Date & Time: 8:30am 20-Sept-2017	Venue: CBY C011		

Group Minutes					
Attendees: Isaak Goldenbergberg igold093@uottawa.ca, Joey Kane jkane035@uottawa.ca, Alex Pennel apenn095@uottawa.ca, Sawyer Woodside swood079@uottawa.ca		Absent:	Date & Time: Sunday, Sept 24th	Venue: Site	
Minute taker: Who is filling out this form?		Chairperson: Who is organising the meeting?			
Task What has to be done?	Action What action is required to get it done?	Who Who is responsible?	Duration How long will it take to complete?	Status Has the task been completed?	
1 Keel desing, Bearing mounting and Batteries selection	Draw sketches of each design concept, being sketches into overleaf file , explain designs	Isaak	2 days		
2 Rack and pinion, position reading, gondola design	Draw sketches of each design concept, being sketches into overleaf file , explain designs	Joey	2 days		
3 friction wheel , communication transmission, timing belt, gondola design	Draw sketches of each design concept, being sketches into overleaf file , explain designs	Alex	2 days		
4 Mounting thrusters to airship, gondola design, keel desing	Draw sketches of each design concept, being sketches into overleaf file , explain designs	Sawyer	2 days		
5					
Next meeting Chairperson: Joey Kane	Minute taker: Joey Kane	Date & Time: Friday, Sept 29th	Venue: CBY		

Group Minutes					
Attendees: Isaak Goldenberg, Igold093@uottawa.ca Joey Kane, JKane035@uottawa.ca Alex Pennell, APenn095@uottawa.ca Sawyer Woodside, SWood079@uottawa.ca		Absent: None		Date & Time: Friday, September 29th, 2017	
Minute taker: Who is filling out this form? Sawyer Woodside		Chairperson: Who is organising the meeting?		Joey Kane	
	Task What has to be done?	Action What action is required to get it done?	Who Who is responsible?	Duration How long will it take to complete?	Status Has the task been completed?
1	Organize and delegate work to all group members	Create an action plan for the modelling report	Joey	1 Hour	Yes
2	Demonstrate final design	Draw sketches of each component in detail	Sawyer	2 Days	No
3	Compute Gondola Reaction Forces	Create free body diagrams and complete static force analysis on gondola parts	Alex	3 Days	No
4	Compute Airship Drag	Create flow simulations in solidworks based on rough dimensions	Joey	2 Days	No
5	Find Thrust Values	Review literature to determine best method of calculating thrust	Isaak	3 Days	No
Next meeting Chairperson: Sawyer Woodside		Minute taker: Sawyer Woodside	Date & Time: Friday, October 6th, 2017	Venue: CBY	

Group Minutes					
Attendees: Isaak Goldenbergberg igold093@uottawa.ca, Joey Kane jkane035@uottawa.ca, Alex Pennel apenn095@uottawa.ca, Sawyer Woodside swood079@uottawa.ca		Absent:	Date & Time: Friday, October 6th	Venue: CBY	
Minute taker: Who is filling out this form?		Sawyer Woodside	Chairperson: Who is organising the meeting?	Sawyer Woodside	
Task What has to be done?	Action What action is required to get it done?	Who Who is responsible?	Duration How long will it take to complete?	Status Has the task been completed?	
1 Gondola Drawings	Draw sketches of each subassembly, how they will be fastened and how they will interact, elaborate in report	Sawyer	5 days		
2 Thruster Support Drawings	Draw sketches of each subassembly, how they will be fastened and how they will interact, elaborate in report	Isaak	5 days		
3 Wiring and Communications	Specify the design, draw sketches of each design concept (wiring diagrams), elaborate in report	Joey and Alex	3 days		
4 Document Tending	Importing Files, formatting, establishing requirements, reworking document template	Alex	2 days		
5					
Next meeting Chairperson: Alex Pennell	Minute taker: Alex Pennell	Date & Time: Friday, October 13th	Venue: CBY		

Group Minutes					
Attendees:		Absent:	Date & Time:	Venue:	
Isaak Goldenberg igold093@uottawa.ca, Joey Kane jkane035@uottawa.ca, Alex Pennel apenn095@uottawa.ca, Sawyer Woodside swood079@uottawa.ca			Thursday, November 2	CBY	
Minute taker: Who is filling out this form?		Isaak Goldenberg	Chairperson: Who is organising the meeting?	Isaak Goldenberg	
	Task What has to be done?	Action What action is required to get it done?	Who Who is responsible?	Duration How long will it take to complete?	Status Has the task been completed?
1	Solve forces on gondola	Code all equations leaving variables adjustable to solve forces acting on gondola	Isaak	5 days	
2	Adjust braking/holding design	Modify braking method in order to not damage and components and ensure efficient braking	All	5 days	
3	Organize Sw files	Begin to set up solid works parts for final design	Sawyer	3 days	
4	Manufacturing method finalizing	Decide on manufacturing methods for each component	Joey	2 days	
5	Set up git hub for coding		Alex	5 days	
Next meeting Chairperson: Isaak Goldenberg		Minute taker: Isaak Goldenberg	Date & Time: Thursday, November 2	Venue: CBY	

Group Minutes					
Attendees: Isaak Goldenberg, igold093@uottawa.ca Joey Kane, jkane035@uottawa.ca Sawyer Woodside, swood079@uottawa.ca Alexander Pennell, apenn095@uottawa.ca		Absent: N/A	Date & Time: 8th of November, 2017	Venue: Isaak Goldenberg's Home	
Minute taker: Who is filling out this form? Joey Kane		Chairperson: Who is organising the meeting? Joey Kane			
	Task What has to be done?	Action What action is required to get it done?	Who Who is responsible?	Duration How long will it take to complete?	Status Has the task been completed?
1	Begin design of final solidworks files.	Solidworks parts and assemblies need to be created, equation based	Sawyer	10 days	No
2	Begin parametrization	Create matlab directories, input equations from modelling report	Alex, Isaak	5 days	No
3	Create LaTeX document	Format document and begin writing section	Joey	2 days	No
4	Redo analysis	Redo some section of analysis report, as well as extra analysis as recommended by the TAs	Joey	3 days	No
5					
Next meeting Chairperson: Sawyer Woodside	Minute taker: Joey Kane	Date & Time: November 15th, 10am	Venue: CBY		

F.2 Team-Partner Meeting Minutes

Team/Partner Minutes			
Attendees: Alex Pennell (apenn095@uottawa.ca,7334789) Isaak Goldenberg (igold093@uottawa.ca,7395188) Joey Kane (jkane035@uottawa.ca,7386330) Sawyer Woodside (swood079@uottawa.ca,7158568)	Absent: none	Date & Time: Sept-15-2017	Venue: C011 and lab
Minute taker: Who is filling out this form?		Chairperson: Who is organising the meeting? Eric Lanteigne	
Minutes			
<p>Discussed overview of the project Wires can cause issues with the system Need to use propellers, since they are more efficient Looked at previous designs Main focus of the project is to design the gondola, other changes to the blimp are extra</p>			
Next meeting Chairperson:	Minute taker:	Date & Time:	Venue:

Appendix G: Recommendations for Improving the Course

lol